Radiochemical studies of the fission of heavy elements by energetic neutrons

Roger Wellum

"Radiochemical studies of the fission of heavy elements by energetic neutrons"

THESIS

presented in candidature for the degree

of

DOCTOR OF PHILOSOPHY

of the

University of Durham

by

ROGER WELLUM, B.Sc. (Dunelm)

MEMORANDUM

The work described in this thesis was performed in the Londonderry Laboratory for Radiochemistry, University of Durham and in the University Chemical Laboratory, University of Kent at Canterbury during the period from 1964 to 1967 under the supervision of Dr. S.J. Lyle, Lecturer in Radiochemistry.

This thesis contains the results of some original research by the author and no part of the material offered has previously been submitted by the candidate for a degree in this or any other university. Where use has been made of the results and conclusions of other authors in relevant studies, care has been taken to ensure that the source of information is always clearly indicated, unles it is of such general nature that indication is impracticable.

ROGER WELLUM.

Roger Wellum

SUMMARY

The cumulative yields for eight selected mass chains from the fission of U^{238} induced by essentially 3 MeV and also 14.8 MeV neutrons have been measured radiochemically. The isotopes counted were Sr^{91}, Y^{93}, Ru^{105}, Rh^{107}, Sb^{129}, I^{131}, Ce^{143} and Pr^{145}. A new rapid chemical separation was devised to enable reliable measurements of yields based on 21.7 minutes Rh^{107}, otherwise existing methods of separation modified were required, where employed in obtaining samples for counting purposes. Radioactive decay of samples was measured using calibrated end-window proportional counters having anticoincidence shielding to reduce the background. Yields were determined relative to that at mass 99 for which values of 6.32% and 5.68% were assumed when employing 3 and 14.8 MeV neutrons respectively.

Masses were chosen so that they provided yields on the wings of the light and heavy peaks in asymmetric fission. It was thereby possible (1) to compare changes

in these regions on changing the bombarding energy of the neutrons and (2) to calculate numbers of prompt neutrons associated with fission-fragment pairs. In this latter connection, decidedly low values were obtained for two fragment pairs from 14.8 MeV fission. The results are discussed in relation to current ideas on the fission process and published experimental results. The yields measured in the course of this work are on the whole complementary to those published for the 3 MeV neutrons induced fission of U^{238}. Their incorporation into the existing yield curve is discussed.

ACKNOWLEDGMENT

I would like to thank the following:

Dr. S.J. Lyle, Lecturer in Radiochemistry, under whose supervision this work was carried out, for his sound advice and constant interest.

Mr. R. Oliver for his technical assistance and for operating the neutron generator.

Dr. C.G.B. Williams for his help in the counter calibration measurements.

The United Kingdom Atomic Energy Authority for financial assistance in the form of a grant for two years and the University of Kent at Canterbury for a Research Assistantship for one year.

My wife for her encouragement and for typing this thesis.

CONTENTS

Chapter I

Introduction

a) Historical

The phenomenon of fission was discovered following the work of Fermi and his colleagues[1.1], who having had considerable success in preparing radioactive isotopes by the irradiation of stable elements with thermal neutrons tried in the same way to produce transuranium elements from uranium. Very soon however, too many radioactive components were identified to be comfortably accounted for by the isomerism of a few elements and furthermore, the chemical behaviour of the elements associated with the activities were different to those expected. A β-active isotope, thought to be that of radium was investigated by Hahn & Strassman[1.2] who showed that it fractionated with barium rather than radium during crystallisation. A second conclusive experiment by Hahn & Strassman[1.3] showed that the daughter activity of the 'radium' isotope crystallised preferably with lanthanum, not actinum as expected.

The interpretation of these results by Meitner & Frisch[1.4] as fission into nuclides of medium mass followed immediately. A review of fission work up to 1940 was carried out by Turner[1.5]. The early discovery of neutrons emitted during fission and therefore the possibility of chain-reactions occuring led to a great deal of work in the field of fission, mainly on U^{235}, during the Second World War in the so called 'Manhattan Project'. The data of radiochemical interest coming from this project have since been published in the National Nuclear Energy series[1.6]. Bohr and Wheeler[1.7] and independently, Frenkel[1.8] proposed a liquid-drop model in 1939 and most fission theories since then have been based on this model.

A great deal of practical and theoretical work has been done since 1946: reviews which summarise much of this material include those of Walton[1.9], Halpern[1.10] and Hyde[1.11]. Useful material is also to be found in the papers presented at the United Nations Conference for the Peaceful Uses of Atomic Energy, held in 1958[1.12].

b) Fission as a phenomenon

The original discovery came from the neutron-induced fission of U^{235} in natural uranium (as predicted by Bohr, 1939,[1.13]) but fission has been observed for nuclei ranging from the heaviest down to copper[1.14].

Mass defect calculations would predict that fission of heavy elememts into two equal fragments is a highly exoergic process. However spontaneous fission is rare for elements of mass lighter than U^{235} (1.8×10^{17}yr) and Th^{232} ($>10^{21}$yr). Spontaneous fission is thought to be an example of quantum-mechanical tunneling, similar to the well-known α-emission tunneling. The spontaneous-fission half-life is then a sensitive measure of the potential barrier to fission which has values lying in the region 5 to 8 MeV for nuclei heavier than radium.

A relation between barrier height and the 'fission-ability parameter', Z^2/A was given by Seaborg[1.15], restricted in this equation to even-even nuclei of a limited range of Z^2/A:

$$Eb = 19.0 - 0.36\ Z^2/A, \quad \ldots\ldots\ldots\ldots\ldots\ldots (1)$$

where Eb is the fission barrier in MeV.

The reaction of a neutron having negligible kinetic energy with U^{235} produces sufficient excitation to take the U^{236} nucleus past the fission barrier, whereas with U^{238}, the main isotope in natural uranium, neutrons with additional kinetic energy of approximately 1 to 2 MeV are needed to cause the U^{239} nucleus to fission to a measurably useful extent.

Nuclei with greater Z^2/A, having lower fission barriers by equation (1) have correspondingly shorter spontaneous-fission half-lives. Examples, listed here in order of increasing Z^2/A are, $Th^{232}(> 10^{21}$ yr$)$[1.16], $U^{235}(1.8 \times 10^{17}$ yr$)$[1.17], $Cf^{252}(85.5$ yr$)$[1.18] and $Fm^{256}(3$hr$)$[1.19].

Nuclei may be excited past the fission-barrier by other means than by neutron bombardment, and fission has been induced by particles ranging from γ-ray photons[1.20] to energetic carbon nuclei[1.21].

As a means of de-excitation for a nucleus, fission suffers competition from α-, n- and γ-emission. Of these, γ-emission is a comparatively slower nuclear process; α-particle emission too is a slow process due to the coulomb

barrier and is only present as an effective competitor, for fissionable nuclei having very long spontaneous half-lives. Neutron-emission however can and does occur within the period of de-excitation by fission. This is of especial importance in the case of moderately highly excited nuclei when the emission of a neutron before fission may still leave the nucleus with sufficient energy to undergo fission.

The equivalent in energy of approximately 200 MeV is released at fission; it manifests itself mainly in the kinetic energy of the fragments. Between 2 to 5 prompt neutrons are also emitted: in this fact lies the possibility of having a self-sustaining system through chain reactions, using neutron-fissile material.

The highly excited fission-fragments have a neutron to proton ratio far removed from stability, which they achieve through, if necessary, successive β-emissions. Nuclear de-excitation of fragments may also occur by γ-emission. This β-γ-emission constitutes the main source of radioactivity from fission.

The immediately formed fragments generally have half-lives short compared to a second and an isobaric chain is formed with the half lives of successive members, as a rule, increasing as the nucleus approaches stability by β-decay.

In a small fraction of events, energetic α-particles are observed. These have an energy spectrum centred at 15 MeV, with a maximum at about 29 MeV. Such events are more correctly classed as ternary fission and they constitute the most common type of ternary fission observed. α-emission, simultaneous with the main fission event has a frequency of occurrence of 0.2 to 0.5%. Angular correlations of the direction of α-particle emission with respect to that of the main fragments show that the α-particle is emitted at slightly less than 90 degrees to the direction of the lighter fragment[1.22]. The liquid-drop model as proposed by Bohr & Wheeler[1.7] envisages the excited heavy nucleus stretching and finally scissioning at a narrow neck during fission. This model gives an attractive explanation of the α-emission[1.23]. The α-particles are assumed to be emitted from the neck at scission, at which time the

coulomb-barrier to α-emission is expected to be low. The direction of emission of the α-particles would then be determined by the competing coulomb repulsions of the main fragments.

A less common form of ternary fission is that of simultaneous triton emission. This has been shown to occur with a frequency of one part in several thousand fission events[1.24, 1.25]. Ternary fission into three sizeable fragments appears to be very uncommon; for example, Rosen & Hudson[1.26] obtained a value of 6.7 per 10^6 binary fissions for U^{235}.

c) Mass-Yields

i) Measurement of mass-yields

The earliest measurements of mass-yields were made radiochemically. Since then, mass-spectrographic methods have added considerably to the amount and the accuracy of the data.

Since β -decay chains are formed, two sorts of fission yield must be defined. The individual amounts of each isotope on the mass-chain formed directly by the

fission process constitute the independent yields, as against the total yield in the mass-chain, which is measured at the stable end of the chain. A measurement of the final stable product or of one of the immediately preceding, long-lived, chain members gives the chain mass-yield.

The radiochemical problem is, briefly, to measure the number of fission events and the number of atoms of a given fission-product isotope. In practise, the measurement of the number of atoms of one given isotope involves (a) the separation of the element radiochemically and in known chemical yield, (b) following the decay, separating the activity from that of interfering radio-isotopes and estimating the activity of the required isotope at the end of the irradiation period, (c) correcting this activity for counter efficiency and self-absorbtion factors and (d) relating the activity to an integrated fission rate over the whole fissioning period. This last requires a knowledge of the fission rate throughout the irradiation.

The strictly radiochemical problem in (a) above, may be solved by separating the active isotopes at the

tracer level and in 100% yield and by counting them by means of an absolute counting method, It is much more convenient however to use macro amounts of inactive isotopic carrier material. The problem then resolves itself into the following stages: (1) the addition of a known amount of carrier to the irradiated sample, (2) ensuring isotopic exchange, if necessary by taking the element through one or more valency changes, (3) the separation of the carrier from all radiochemical impurities and (4) following the decay using a suitable counter. Chemical yields are then determined directly from the weight of the solid source or by measuring the amount of the stable isotopic carrier in the source after all activity has died away, by whatever analytical methods are most appropriate for the sample.

The determination of the absolute number of fissions is a difficult one experimentally. However it is in part circumvented by measuring the yields of the isotopes required against one fission-product as a reference. These relative fission yields must then be converted to absolute yields. One method, and the simplest if applicable, is to

multiply the relative yields by the absolute yield of the reference isotope. This requires of course, the knowledge of the reference isotope in this fissioning system. Obviously the accuracy of the absolute yields of all mass-yield points are only as accurate as the estimation of this absolute yield.

An alternative method is to make use of the fact that nearly all fission events are binary events. After allowing for the prompt neutron emission a plot of relative fractional mass-yield against the mass number of the fission fragment may be adjusted until the integrated yield measured under the curve adds up to 2. Provided sufficient relative mass-yield points are known to outline the shape of the curve, the adjustment only involves altering the yields by a constant factor. This method is made possible in practise by the sharp tailing off at high and low masses: then provided the peaks are well-defined, little error ensues from ignorance of low-yield points at the extremities of the curves.

If the measurement of chain-yield is made with an

isotope part way along the chain - and the consideration of which isotope to use in the chain is usually determined by experimental comditions such as half-life or decay characteristics - then the independent yields of isotopes later in the chain must be allowed for. This requires a knowledge of the charge distribution along the mass-chains.

A theory relating to charge-splitting between the primary fragments in nuclear fission is not at present available. Early conjectures, that the fission-fragments have charge to mass ratio identical to the fissioning nucleus or that the charge division occurs so as to give maximum kinetic energy to the fragments and minimum to radioactive decay do not agree with the observation that the decay chains for the heavy and the light fragments have approximately equal lengths.

Glendenin, Coryell & Edwards[1.27] put forward the empirical hypothesis that the most probable charges for the light and the heavy fragments lie an equal distance from beta stability. The charge distribution is further postulated to be Gaussian about the most probable charge position along the β-decay chain.

From the equal charge displacement hypothesis it follows that if Z_A, Z_A^* are the stable charges of each fragment and Zp, Zp^* are the most probable charges, then

$$Z_A - Zp = Z_A^* - Zp^*$$

and since $A + A^* = A_f - \nu$

where A and A^* are the fragment masses, A_f that of the fissioning nucleus and ν the number of prompt neutrons emitted, then

$$Zp = Z_A - \tfrac{1}{2}(Z_A + Z_A^* - Z_f).$$

The distribution curve has the form

$$P(Z) = \frac{1}{\sqrt{C\pi}} \cdot \exp\left(-\frac{(Z - Zp)^2}{C}\right)$$

where P(Z) is the probability of obtaining a charge Z relative to that of the most probable charge Zp. c is an empirical constant.

Formulations for Z_A are required to make these equations useful in practise. In the treatment of Glendenin, Coryell & Edwards, the Bohr-Wheeler mass equation was used giving a smooth Z_A function with

fission-product mass. Pappas[1.28] altered the Z_A function to take into account discontinuities at shell edges and Kennett & Thode[1.29] made further adjustments to account for their measurements on Xe^{128}, Xe^{130}, Xe^{131} by accurate mass-spectrometric techniques.

These various formulations were in effect superceded when Wahl[1.30] published his work on independent yields from U^{235} together with all other available data; by fitting a Gaussian curve similar to that used by Glendenin, Coryell & Edwards[1.27], about the independent yield points, he determined the value of Zp for each mass-chain for which there was sufficient information.

(ii) Mass-yield curves

The mass chain-yield distribution for U^{235} has been extensively studied for thermal neutron induced fission. The data has been collected by Katcoff[1.31]. The obvious striking feature of this curve is the marked asymmetry of the chain-yields with respect to mass of the fission-product nuclei; it is centred about masses 95 and 138, approximately. This asymmetry in fission had first been.

demonstrated by Jentschke & Frankl[1.32] who measured the kinetic energies of fission fragments and found they lay around two bands centre at 60 MeV and 100 MeV. Confirmation of the associated mass-asymmetry closely followed and this phenomenon is now generally accepted as a characteristic of low-energy fission.

The asymmetry of the mass-yield curve may conveniently be defined by the ratio of fission yields on the peaks of the mass-yield curve to that in the trough (the so called 'peak to trough ratio').

An obvious experimental result of increasing the excitation energy is to lower the peak to trough ratio: between thermal fission and fission with 14 MeV neutrons, the peak to trough ratio varies from about 600 to about 60 with U^{235} - a variation by a factor of ten[1.31].

As might thus be expected, spontaneous fission yields have the greatest peak to trough ration in accordance with their very low excitation energy. Work has mainly been done on the heaviest available nuclei as these have workable spontaneous fission rates, and very low symmetric yields for

Cm^{242} 1.33 and Cf^{252} 1.34 have been observed.

Fission yields produced from highly excited nuclei have a single peak, but with broad wings suggesting a still extensive contribution from asymmetric fission. A study of high energy proton fission by Stevenson et al[1.35] on U^{238} shows the double peak, still evident at a bombarding energy of 10 to 30 MeV, merge with the filled-in centre portion to present a single broad curve at 200 to 300 MeV. It is significant that at these energies the best fit hypothesis of charge distribution is that which allows the fission-fragments the same charge/mass ratio as the parent nucleus.

A variation in the form of the mass-yield curve is observed with change in the mass of the fissioning nucleus. In particular elements of mass lower than that of thorium have frequently given differently shaped curves compared to those of heavier masses. Thus Fairhall[1.36] observed a single, narrow peak for bismuth bombarded with 16 MeV deuterons. With increasing excitation energy this peak broadens: a single much broader peak was observed by Goeckermann & Perlman[1.37] using 190 MeV deuterons.

Intermediate behaviour between single-humped, symmetric fission and double-peaked asymmetric fission was found by Jensen & Fairhall[1.38]. They found that radium with 11 MeV protons gave a three-humped mass-yield curve. They concluded that two distinct types of fission were being simultaneously observed.

This intermediate case, where the symmetric mass-yield is comparable to the asymmetric yield is rare and has only been observed for light elements at moderate excitation energies. Other systems that have shown a three-humped yield curve are U^{233} bombarded with helium ions between 25 and 40 MeV[1.39], Th^{232} with 3 MeV neutrons[1.40], and Pa^{231} with 14 MeV neutrons[1.41].

The two mode hypothesis of fission has received experimental backing from kinetic energy studies on fragments and from prompt-neutron emission studies.

Measurements on the kinetic energy of fragments produced by the thermal-neutron induced fission of U^{235}, by Apalin et al[1.42] confirmed earlier energy measurements

by Milton & Fraser[1.43, 1.44] who observed that asymmetrical fragments have kinetic energy in excess of symmetrical fragments of about 20 MeV. The argument that follows from these observations is that if symmetric and unsymmetric fission require similar excitation energies to occur then the missing kinetic-energy of the symmetric fragments appears in the form of deformation energy or nuclear excitation energy. The fragment kinetic energy measurements have been paralleled by studies of the number of prompt-neutrons emitted in association with individual fragments. The now familiar saw-tooth distribution for the number of prompt-neutrons plotted against fragment mass $\nu(m)$, was shown by Terrell[1.45] by collating radiochemical and fragment yield data for U^{235} U^{233} and Pu^{239} and observed directly by Apalin et al[1.46, 1.47]. Earlier work by Stein and Whetstone[1.48] had shown the same characteristic neutron emission curve as a function of fragment mass for C_f^{252}. Recent measurements of $\nu(m)$ by Milton and Fraser[1.49] for U^{235} confirming the shape of the curve have also shown fine structure — minor peaks in the yield of $\nu(m)$ at masses 90, 96, 101.

Measurements made by Milton & Fraser[1.49] and Apalin[1.46, 1.47] are velocity or energy measurements of the primary fission fragments at about the time of prompt-neutron emission. Mass-yield curves are constructed from their data simply by applying the laws of conservation of momentum and energy. These curves then differ from radiochemical mass-yield curves by the prompt-neutron emission of the fragments and the β -decay of the chains.

One major difference between mass-yield curves constructed from fragment energy data and radiochemical data is the presence of abnormal yields with respect to a smooth curve in the radiochemical case. Mass-spectrometic measurements by Thode & co-workers[1.50, 1.51] on the abundances of krypton and xenon isotopes in the thermal neutron induced fission of U^{235} showed in particular a high yield of Xe^{134} over that expected from a smooth curve. Fine structure in mass-yield curves has since been obtained for several fission systems. It is of most significance for low energy fission and becomes less pronounced as the excitation energy is increased[1.51, 1.53].

The first explanation for fine structure was suggested by the position of the most significant fine structure around mass 134. The closeness of this peak to the closed neutron shell of 82 neutrons led Glendenin[1.54] to propose that fission fragments having a slight excess of 82 neutrons would preferentially boil off neutrons to yield this shell. Wiles[1.55] on the other hand suggested that a fission fragment with 82 neutrons would be preferentially formed during the fission act.

A second explanation, put forward by Farrar[1.56] and independently by Terrell[1.45] linked the variation in prompt-neutron emission as a function of fragment mass with the fine structure. Changes in $\nu(m)$ could well account for increased yields at particular masses and the effect would be displaced in the two cases by the length of the β-decay chains.

This explanation is attractive in as much as sufficient structure has been observed to account for the required mass-structure. Fragment mass-yield curves as measured by the time-of-flight technique of Milton & Fraser[1.43, 1.44, 1.49] have distinctly different detailed

shapes as compared to the product yield curves. Structure is present but it is less pronounced than that observed in the product yield curves. These fragment mass-yield curves are symmetrical about the lowest point in the trough. This contradicts Wiles postulate[1.55] that shell effects preferentially pre-select certain fragment masses.

A characteristic of fission mass-yield curves whenever the presence of asymmetric fission is observed is the constancy of the position of the light wing of the heavy peak. This applies to cases as far-apart as spontaneous fission of Cf^{252}, 11 MeV proton induced fission of Ra^{226} and 14 MeV neutron induced fission of U^{238}. (See for example ref.[1.56]). Such an effect suggests a common cause in each of these cases determining the position of the peak itself or the inside edge of the peak. The occurence of the doubly magic nucleus of mass 132 ($N = 82$, $Z = 50$) must then be more than mere coincidence. With changes in the fissioning nucleus, the light peak moves to keep the sum of the masses of the fragment pairs equal to that of the parent nucleus after prompt neutron emission.

d) Theoretical models of the fission process

Any theory of fission has several outstanding experimental observations to explain: These have been listed by Ramanna[1.57] as follows:

a) The strong asymmetry of the mass distribution in low and medium energy fission and the variation of the asymmetry/symmetry ratio with excitation energy.

b) The approximate constancy of the fission barrier for many heavy nuclei at about 5 to 7 MeV.

c) The prompt-neutron saw tooth curve with mass number and the correlation of neutron-emission with fragment kinetic energy.

d) The odd-even behaviour of the spontaneous fission half-lives.

Swiatecki has pointed out the basic existence of the liquid drop model in all fission theories whether they are based explicitly or not on the model[1.58]. Depending on the assumption as to whether the collective modes of motion of the nucleus as a whole are strongly or weakly linked to those of the individual nucleons the statistical or the adiabatic model are derived.

The adiabatic approach has been linked very closely with the liquid-drop model as developed by Swiatecki and co-workers. A great deal of effort has been put into determining the static potential of energy surfaces of deformed nuclei. The biggest problem in the case of the simple liquid-drop model has been the lack of explanation for the asymmetry yields in fission. Work in calculating possible modes of deformation in heavy nuclei has therefore always been directed towards the possibility that certain deformations and therefore the forms of fission would be asymmetric in character.

The statistical approach associated with Fong[1.59], concentrates on the nucleus at the moment of breaking up. By considering that all modes of fission are possible due to the proliferation of fission channels at the highly excited scission point the products actually formed will depend on their relative stabilities. Fong obtained results in good agreement with observed mass-yield values in the case of U^{235} but his approach has had difficulties in other cases in reproducing observed results.

Both the adiabatic and the statistical approach are obviously only partial in their attempts to cover the fission process. We may consider fission as taking place through the excitation of a nucleus to a saddle-point - that energetically required to cause fission - then a re-arrangement of the nucleus by collective or individual movements to the scission point followed by the actual occurence of scission. It is apparent that the adiabatic model concentrates on the period up to the saddle-point and the statistical model on the period at the scission point.

Other work has been done, which although not along the same direct lines as the two previous models has thrown light on the fission process. A. Bohr in his paper[1.58] on the liquid-drop model as applied to fission showed that nuclei excited just to the fission barrier would be in a 'cold' state at the saddle-point. In particular there follows the chance of linking the excited states of this nucleus, by analogy, to ground states.

Concentrating on the period between the saddle-point and scission, Ramanna [1.57], treating the process

stochastically obtained the basic yield curves for several cases. He assumed that the fragments slowly separate and a free interchange of neutrons occurs up to scission; the protons were considered to be fixed relatively early in the process by the coulomb forces which build up. Shell effects which tend to hold or stabilise certain numbers of neutrons were included in the treatment.

Along similar lines, Faissner and Wildermuth[1.61], considered stabilisation effects by applying cluster theory considerations to the neutron and proton shells of the fission fragments before scission. The pre-existence of clusters containing N = 50, N = 82 and Z = 50 nucleons emphasizes in particular the role of the A = 132 double shell, (N = 82, Z = 50), in determining the positions of the heavy peaks. For the lighter peak, as there are several choices of combinations of proton and neutron shells, the actual contribution of each shell, which is unknown, may be varied to obtain the best fit to experimented results. This availability of adjustable parameters detracts from the usefulness of the procedure. However it is pointed out by Faissner that closed shells will be associated with low

excitation energies and are therefore susceptible to experimental verification of their existence during the fission process.

Vandenbosch[1.62] also dealt with the effect of closed shells being present during fission. He emphasized that closed shells have spherical, undeformed structures. At the moment of scission then, if we consider a near-symmetric splitting of the fragments, the heavier one, lying near the N = 82, Z = 50 closed shells will have a comparatively rigid spherical structure. The excitation energy of this fragment will therefore be mainly as kinetic energy. The lighter fragment, having no closed shells will be highly deformed and have correspondingly less kinetic energy. Reversing the case and taking an example of highly asymmetric splitting, the heavy fragment is expected to be the farthest away from a closed-shell structure and will therefore be the more deformed of the two fragments.

These arguments give a convincing explanation for prompt neutron emission and fragment kinetic energy characteristics with respect to fragment mass. Prompt

neutrons would be expected to be preferentially emitted from deformed nuclei.

The work cited above shows the importance attached to shell effects in determining the gross shapes of the mass-yield curves, in particular the N = 82, Z = 50 shells in fixing the position of the heavy peak. Meitner[1.63] has pointed out that for fissioning nuclei having fewer than 132 neutrons, asymmetry is not observed. These nuclei cannot provide the 82 and 50 neutron shells to stabilise the heavy and the light peaks and so the modes which have the greater transition probabilities of occuring in the excited nuclei at the saddle-point, namely the symmetric modes, are found.

e) <u>The purpose of the present work</u>

The availability of 3 MeV neutrons in reasonable intensities from the Cockroft-Walton linear accelerator at the University of Kent at Canterbury raised the possibility of the investigation of mass-yields for U^{238} bombarded by neutrons of an energy more closely defined than that of 'fission-spectrum' neutrons.

Mass yields for U^{238} excited with fission-spectrum neutrons have been collected and renormalised by Walker[1.64]. Measurements published up to 1961 are included in this review. Since then, values for several mass-yields for this system have been published by Bonyushkin et al[1.65] and Petrzhak[1.66].

Results of mass-yield determinations for U^{238} fission at three initial neutron excitation energies were summarised by Hemmendinger[1.53]. His smoothed mass-yield curves suggest that with increasing excitation energy the heavy peak moves to a lower mass position, whereas the light peak position remains relatively fixed. It has also been observed that the position of the heavy peak maximum obtained in the fission of Th^{232} with 14 MeV neutrons was at lower mass than that reported for thorium fissioning at lower excitation energies. This trend was confimed by the observations of Rahman[1.67] who carried out careful yield measurements for Th^{232} bombarded with 3 and also 14 MeV neutrons.

The present work was directed at measuring mass yields from U^{238} excited with 3 MeV neutrons.

This was in order to give more information at masses whose yields had not previously been measured experimentally. It was also thought useful to repeat the measurements for the same masses for fission of U^{238} bombarded with 14 MeV neutrons to assist in comparing the movements of the peaks at the two excitation energies. By choosing masses on the steep slopes of the peaks, their actual positions might be more closely defined through their centroid masses than by measurements made near the top, where fine-structure effects are apparent. Mass yields measured on the steep parts of the curves also lead to a value of ν, the number of prompt neutrons emitted by complementary fragments. The work carried out in pursuit of the objective is set out in the subsequent chapters of this thesis.

Chapter 2

Experimental Techniques and Instruments

a) Experimental Procedure.

The isotopes employed and their nuclear characteristics are discussed in the next chapter. The same irradiation procedure was used in all cases although the lengths of the irradiations were varied from ten to ninety minutes depending on the isotopes to be separated and the bombarding neutron energy employed.

The sample of uranyl nitrate was sealed in polythene, positioned behind the target of the S.A.M.E.S. accelerator at the University of Kent at Canterbury and irradiated. The neutron flux was monitored throughout the irradiation. The time at the end of the irradiation was noted and the sample was left sealed for a specified period to allow precursor isotopes to decay. The sample was then transfered from the polythene container and dissolved in water or dilute acid. Accurately measured amounts of inactive carriers were added for each element it was proposed to separate. The solution was heated and an oxidation-reduction cycle or other appropriate chemical reaction performed to ensure isotopic exchange had occurred.

Chemical separations were then carried out, each element finishing radiochemically pure as a precipitate. The precipitates were mounted on glass-fibre discs, dried and weighed. Each source was then counted in the same, previously calibrated end-window, beta-proportional counter until sufficient data had been collected to enable its activity at the end of the irradiation to be estimated within the required accuracy limits.

The chemical efficiency was determined for each source, from its weight soon after preparation or from the results of analyses carried out on completion of the counting.

Measurements which were necessary for the calculation of relative yields are the activities at the end of the irradiation, the efficiencies of chemical separations, the self-absorption or counter efficiencies and the variation of the fission-rate throughout the irradiation as indicated by the monitor readings. These measurements were made for the reference element as well as for the isotopes under investigation.

A full description of these measurements as performed experimentally in this work is found in this and the following chapter.

b.) The neutron sources and irradiation techniques

i) 3 MeV neutrons

A S.A.M.E.S. (Societe Anonyme de Machines Electrostatiques, Grenoble, France) 400 kV 'T' type accelerator was employed to produce essentially 3 MeV neutrons by the reaction

$$H^2(d,n)He^3 + 3.266 \text{ MeV}$$

This machine has been well described by previous workers[2.1, 2.2] and needs only a brief description here.

A rotary Van der Graaf electrostatic voltage amplifier excited deuterium ions up to 400 kV by a series of electrodes along the accelerator tube. The deuterium ions were produced by radio-frequency excitation at an ion source and after acceleration were focussed electrostatically through a drift-tube extension on to the target mounted in a separate room from the main accelerator.

The target was a segment cut from a titanium deuteride disc obtained from the Radiochemical Centre, Amersham. The titanium was supplied mounted on a copper disc. This

was soldered carefully on to a water-cooled metal block. As energy of about 400 watts were deposited in the target during irradiations, a supply of cooling water was passed behind the target to ensure that its temperature remained low thereby minimising loss of deuterium from the target. The arrangement of sample, target and coolant is shown in figure 2.1.

The sample, generally about 10 grams of uranyl nitrate, was compressed into a disc, 2cms in diameter by approximately 1 cm thickness. This was placed in a thin polythene envelope which was sealed with a rubber band. The sample package was held in position on the target block of the accelerator with large rubber bands.

Typical beam currents obtained were about 700 μA at an accelerating voltage of 400 kV. The neutron fluxes for such runs were approximately 5 x 10^8 n/cm^2/sec. The neutron fluxes kept reasonably steady during irradiations although breakdowns through electrostatic discharges to the walls of the building from the high potential electrodes were fairly common. The flux was monitored by a solid-state counter, ORTEC model no. SBJ007-60, which counted

Target arrangement for producing 3 MeV neutrons

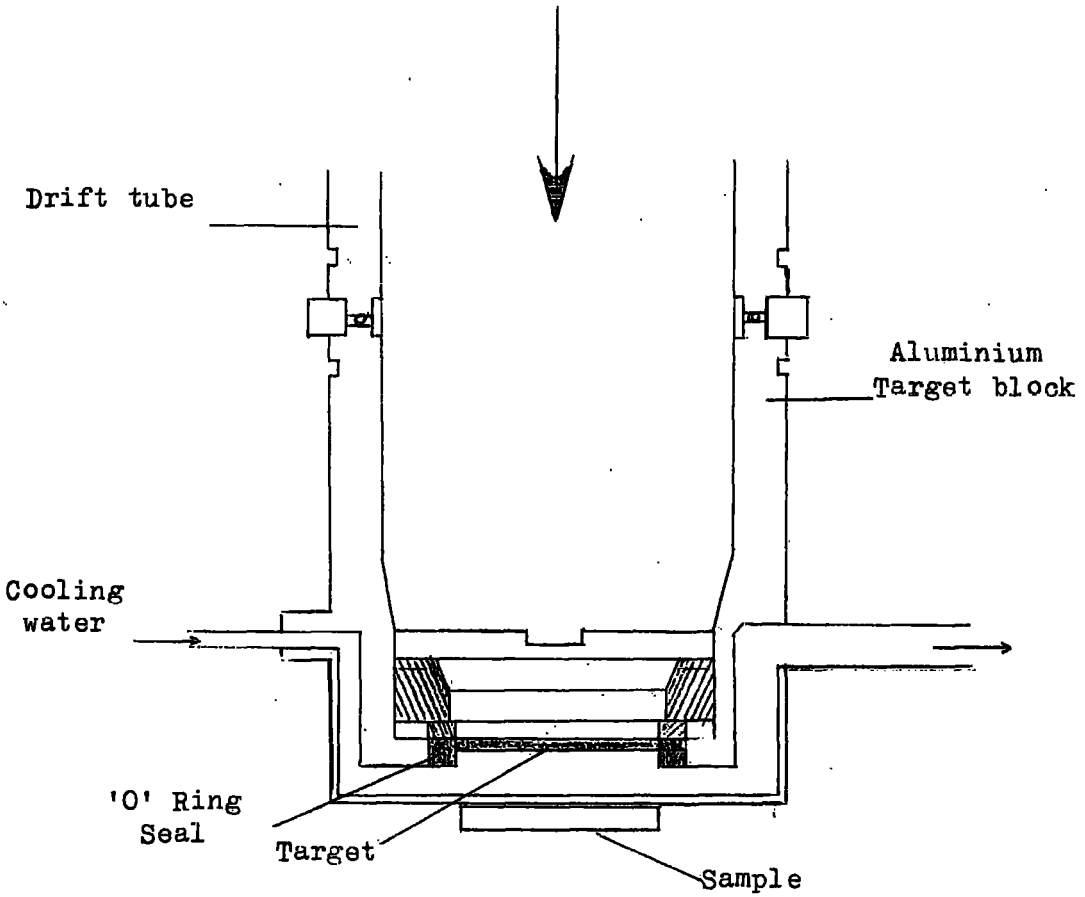

Figure 2.1

the protons produced by the $H^2(d,p)H^3$ reaction.

The energy of the neutrons produced by the accelerator with the operating conditions described has been estimated to be 2.9 ± 0.4 MeV[2.3].

ii) 14 MeV neutrons

The S.A.M.E.S. accelerator was again utilised for the production of 14 MeV neutrons. A tritium target as described by Wilson and Evans[2.4] produced neutrons by the reaction $H^2(t,n)He^4 + 17.58$ MeV. This reaction has a larger cross-section than that of the $H^2(d,n)He^3$ reaction and deuterons of energy only about 110 kV were required. The cooling requirements were correspondingly less severe and the cooling water was passed around the target, not between the target and the sample.

The energy of the neutrons produced on the S.A.M.E.S machine by the $H^2(t,n)He^4$ reaction has been estimated to be 14.8 ± 0.2 MeV[2.2].

During irradiations the neutron fluxes fall off due to loss of tritium from the target. A competitor to the

$H^2(t,n)He^4$ process is the $H^2(d,n)He^3$ reaction arising from deuterium from the beam accumulating at the target. This has been shown to introduce an error of not more than 2% for mass-yield measurements made on U^{238} fission[2.5]. To minimise this effect however, only the first half of the total useful life of the titanium tritide targets was used in these experiments.

It was found that due to the higher fluxes and improved geometry of the sample position relative to the target, quite sufficient activities were obtained from two or three grams of uranyl nitrate, loosely packed in a polythene finger and closed in with a rubber band, after irradiations of ten minutes.

c) Counting equipment

The solid beta-sources, prepared as described in section d), were counted using end window proportional counters constructed of brass in this laboratory (figure 2.2). The design was such as to minimise their height so that an anti-coincidence Geiger shield could be constructed with reasonable dimensions about the counters. The 1mg cm^{-2}.

End-window Proportional Counter

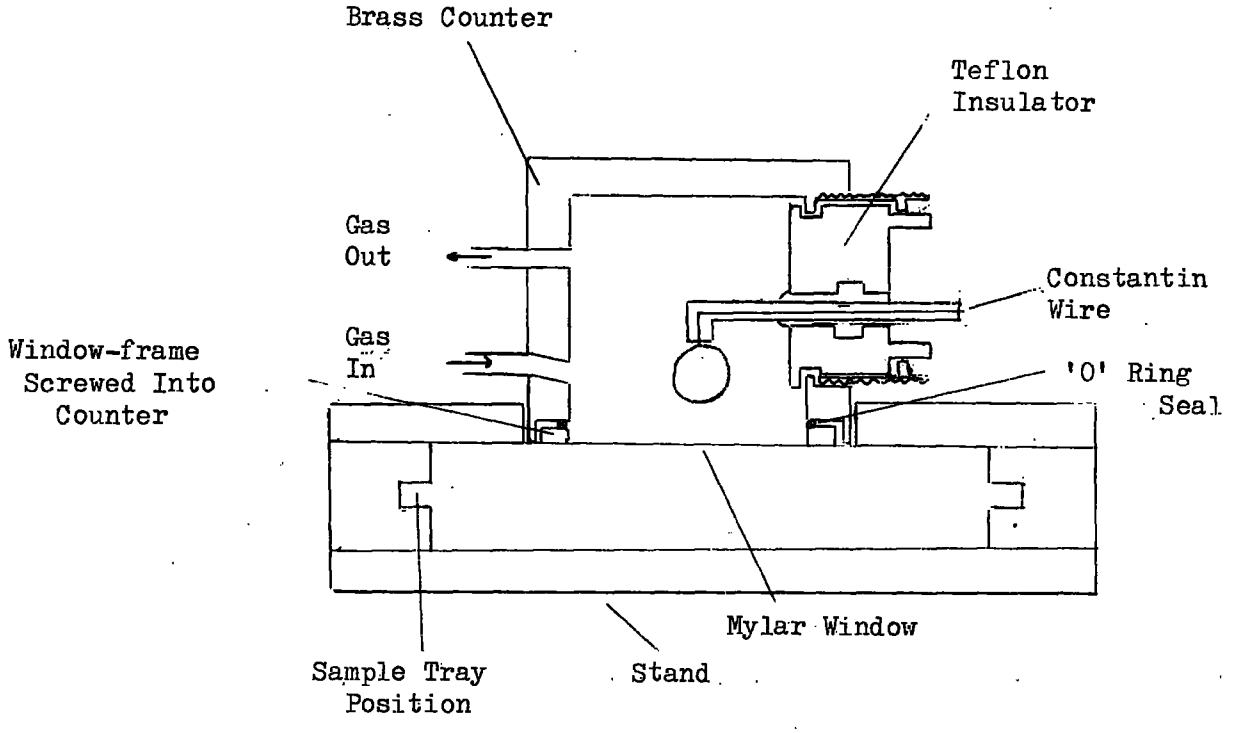

Figure 2.2

aluminised 'mylar' windows had sufficient mechanical strength to allow two or more counters to be linked in series to the same gas supply.

The counters were supplied with a standard 90% argon - 10% methane gas mixture from a cylinder (British Oxygen Co. ltd). The gas was dried by passing it through tubes of magnesium perchlorate and silica gel, filtered through glass wool and finally passed through a reducing valve and flow-meter. Slight alterations in the gas flow above a certain minimum value had no discernible effect on the counter characteristics.

The counting arrangement is shown in figure 23. An anticoincidence low-background system was used to enable accurate counting statistics to be obtained at the low count rates encountered with long-lived isotopes produced in the 3 MeV irradiations. It consisted of a ring of twenty one 20th Century Geiger tubes, type G24, surrounding the proportional counters but allowing direct access for the source trays to be slipped into the holders. The pulses from the proportional and Geiger counters were fed after

The End-Window Proportional Counter, Electronics and Gas Supplier.

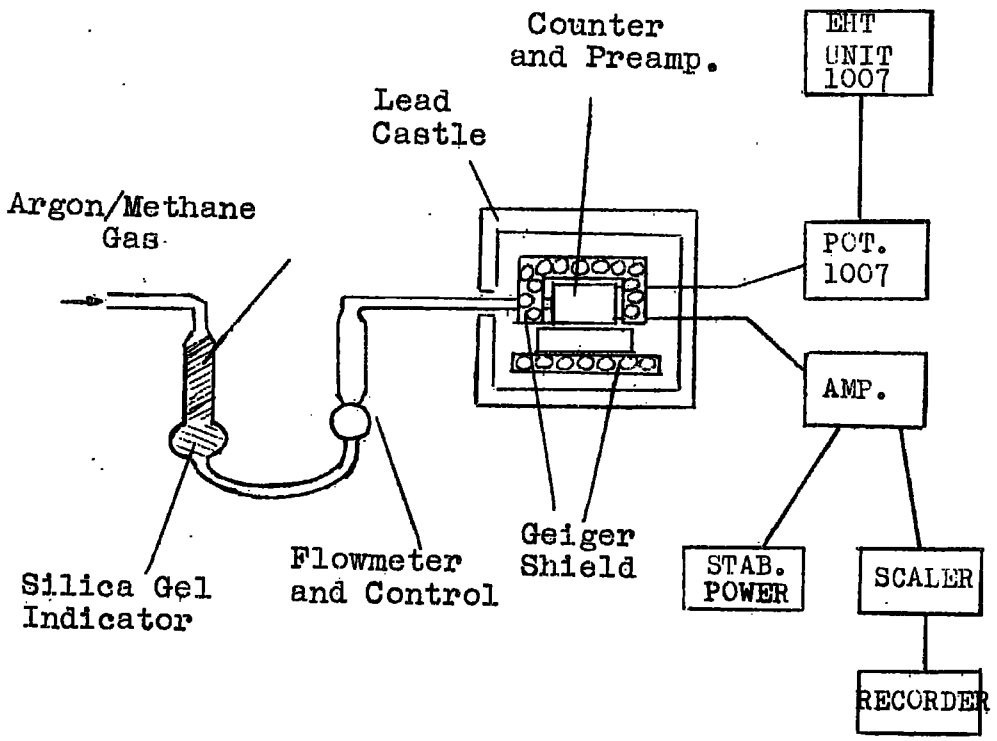

Figure 2.3

amplification to an anticoincidence unit. Pulses from the proportional counter in coincidence with those from the Geiger counters were rejected. The effect was to reduce the background due to cosmic rays, normally between 9 to 11 counts per minute when the proportional counter without coincidence was mounted in a lead castle to between 2.5 and 3.5 counts per minute. A block diagram of the anti-coincidence electronics is shown in figure 2.4.

The amplifiers for the proportional counters were based on the design of Chase and Higginbotham[2.6], modified to take Kandiah output discriminator circuits[2.7]. The preamplifier stages were separated from the main amplifiers and were mounted directly on the counters. This arrangement reduced the noise of the system by minimising the noise originating before the preamplifier - which may often be the main source of noise in high gain amplification systems as used with proportional counters.

The preamplifiers were designed small enough to fit inside the Geiger shield.

Plateaus of three to four hundred volts in length

The Arrangement of the Electronics for Anticoincidence Counting

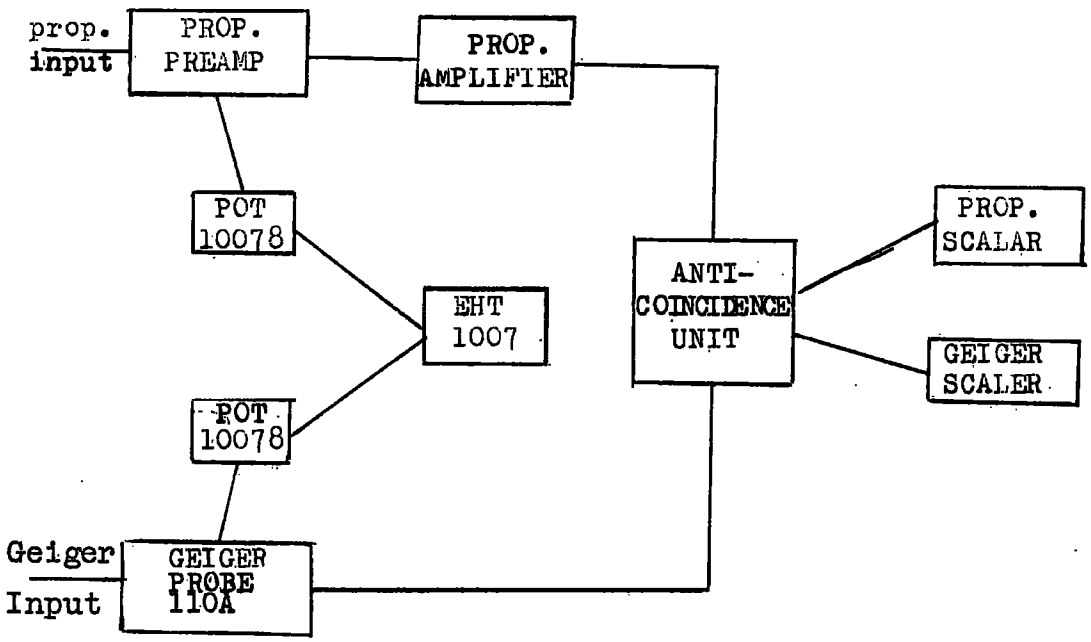

Figure 2.4

were obtained using the arrangements described. Counting was carried out at about 1700 volts. A standard source was used to check the long-term counter stability and a weekly check was made on the plateaux positions.

An automatic recording device was used to extend counting periods overnight. The dead-times of the amplification systems were fixed at 200 μs. This value was chosen as a convenient mean between that determined by the scaler dead-time (which was the largest individual dead-time of any part of the system) and that required to prevent needlessly large dead-time corrections at high count rates.

Two nearly identical proportional counters were used in this work. Each isotope was counted in only one of them however and both counters were calibrated as described in part e).

The counter efficiency measurements made use of a 4π- β - counter to measure absolute disintegration rates. This was a β - proportional, gas-flow counter having a double anode configuration (figure 25). The active material was deposited on very thin ($15 \mu g.\,cm^{-2}$ thickness)

4π Proportional Counter

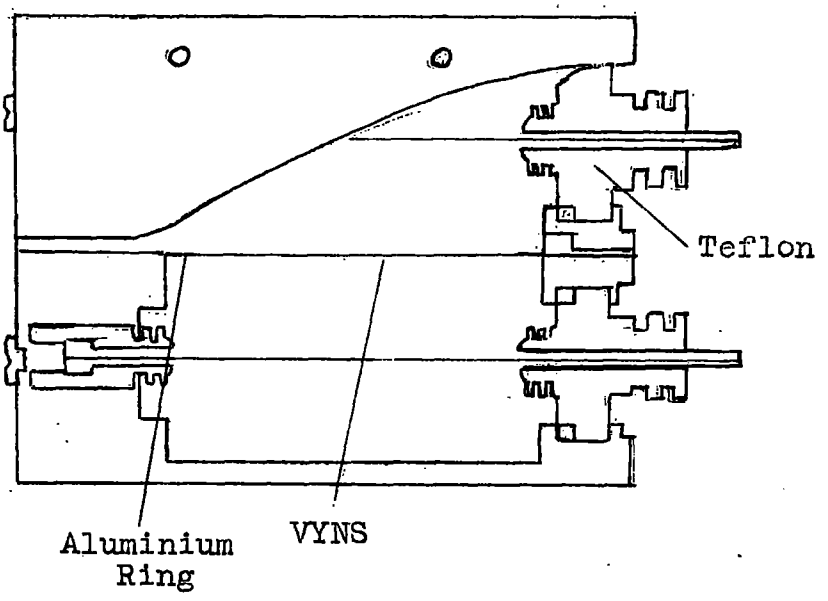

Figure 2.5

V.Y.N.S. film which had previously been coated with about 5μg cm^{-2} of gold on one side by vacuum sputtering to render it electrically conducting. A drop of insulin solution (about 0.1mg per ml) was placed on the film beforehand and dried. This method, described by Pate and Yaffe[2.8], ensured that the active material was evenly spread over the centre of the film. Amplifier and preamplifier types 1430-A were used for the 4π counting.

d) Preparation of solid sources

As explained in chapter 3, not all the elements whose relative yields were measured could be precipitated in a form suitable for weighing in order to determine their chemical yields gravimetrically. Precipitates which were considered suitable for mounting were those which gave well-defined sources and which did not contract and fissure badly on drying. Precipitates such as molybdenum 8-hydroxyquinolate became more suitably granular when boiled with a very little detergent present as a surface activator. Others, such as palladium (II) iodide, required rapid filtration from cold solution to prevent 'clumping'.

The sources were mounted on Whatman GF/A glass-fibre discs, 2cm in diameter, which had previously been washed with water and acetone. The sources were either dried to constant weight in an oven at 120C or were vacuum dried after washing with alcohol and ether. The treatment depended on the particular precipitate.

Few of the sources showed any changes in weight over a period of weeks. As an example, the molybdenum 8-hydroxyquinolate sources when reweighed up to a month after precipitation showed typically no more than a 0.01 or 0.02 mg change. Weighings were made with a Stanton semi-micro balance (model M.C.I.A.) to the nearest 0.01mg.

The sources were prepared using a Hahn type filter-stick, made entirely from polythene. A sintered polythene disc, slightly larger than the glass-fibre filter disc it supported, fitted into a recession in the top of the lower half of the stick. The upper half fitted into this recess and held the filter disc firmly in place around its edge. The precipitate was poured as a slurry into the upper half of the filter-stick and the liquid drawn through by suction. After washing the precipitate, typically with distilled

water and acetone or water, alcohol and ether, the suction was stopped, the filter-stick dismantled and the glass-fibre disc carefully transfered to a planchette. The planchettes were of aluminium, 2.2 cm in diameter, which accurately fitted the central hole of the source tray. The source trays fitted smoothly into the shelving arrangement shown in figure 2.2. This arrangement ensured that the source-counter geometry remained constant. An aluminium backing plate, approximately 0.5 cm thick, was fastened to the back of the sample tray. The saturation beta-particle backscattering from this plate gave slightly higher counter efficiences than would otherwise have been obtained.

e) Measurement of Counter Efficiency

The efficiency of a counter is defined for any isotope, as the ratio of the number of events recorded by the counter to the number of disintegrations which occured in the sample during that period. The geometrical position of the sources with respect to the windows of the proportional counters together with beta absorbtion in the sources and the counter

windows were the main factors which limited the efficiences of the counters to about 35%.

Self-absorbtion of the β-rays in the sources themselves meant that the counter efficiences were determined to some extent by the source weights. Plots of counter efficiences versus source weights were therefore needed for each isotope counted.

The determination of the self-absorbtion plots was carried out with the cooperation of several members of this laboratory: the method used was that of Bayhurst and Prestwood[2.9].

Their prescription calls for a series of self-absorbtion plots to be made for several isotopes whose β-spectra are known. A mean beta energy is calculated for each component in the β-emission spectrum of the isotope. (Corrections are applied for forbidden transitions in this calculation.) The components are weighted according to abundance and averaged for the isotope. The final average mean energies are plotted against counter efficiency for each of the source weights: 5, 10, 20, 30 and 40 *mg* were

used in the work conducted in this laboratory. Sample curves obtained using this method on one of the counters are given in figure 2.6.

For isotopes having an unknown counter efficiency, the reverse procedure was adopted: the mean energy for each maximum β-energy was computed and the corresponding counter efficiences determined from the Bayhurst-Prestwood calibration curves previously constructed. The counter efficiency for the whole beta-spectrum of the isotope was then calculated at each standard source weight by averaging the efficiences weighted according to their respective beta abundances and the self-absorbtion curves plotted.

The isotopes used to calibrate the counters were Ca^{45}, W^{181}, I^{131}, Na^{22}, Au^{198}, Na^{24}, Y^{91}, Y^{90} and K^{42}, listed here in order of increasing mean β-energy. Of these, Na^{22} and Au^{198} were determined absolutely by $4\pi-\beta-\gamma$ coincidence methods and the remainder by absolute $4\pi-\beta-$ counting.

Each standardisation required an active solution as free from inactive isotopic material as possible to be

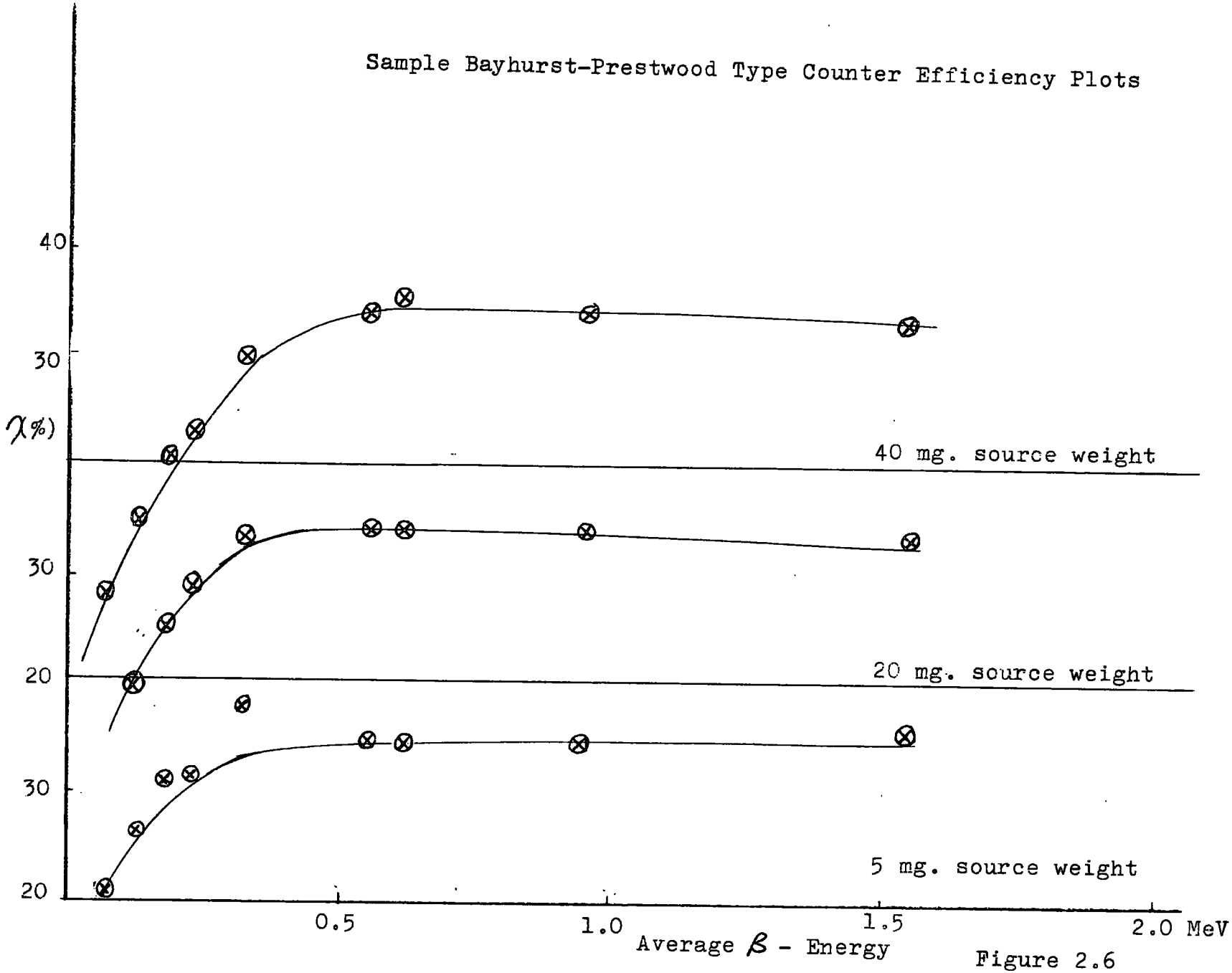
Sample Bayhurst-Prestwood Type Counter Efficiency Plots
40
30
χ(%)
40 mg. source weight
30
20
20 mg. source weight
30
20
5 mg. source weight
0.5
1.0
1.5
2.0 MeV
Average β - Energy

Figure 2.6

calibrated by an absolute counting method. A known weight of the standardised solution was then mixed with a measured quantity of inactive isotopic carrier material and a series of sources from 2 to 50 g. were prepared. The ratio of the activity of each source measured with the endwindow proportional counter to that calculated from the activity known to be associated with the source gave the counter efficiency for each source weight.

Checks on the accuracy of the above method for isotopes for which the counter efficiences had been independently determined by $4\pi-\beta$ absolute counting have been made in this laboratory[2,10]. The results agreed within 2 to 3%.

Several of the isotopes whose relative yields were measured had a daughter activity in equilibrium. The daughter made a contribution to the effective counter efficiency and a correction had to be applied.

Two separate cases occured in this work. In the first the beta energies of parent and daughter isotopes were known: a relation between the absolute activity of the parent, the observed equilibrium activity and the counter

efficiences of the counters for the two isotopes was required. In the second case an efficiency for the mixture was known and a relation between this, the absolute parent activity and the observed activity was needed.

If A, I and η are the absolute, the observed activities and the counting efficiency for any isotope or mixture of isotopes, and if we designate the parents by the subscript '1', the daughter by '2' and the observed cases by 'o' then

$$A_o = A_1 + A_2 \quad \text{----------(1)}$$

$$I_o = I_1 + I_2 \quad \text{----------(2)}$$

$$I = A.\eta \quad \text{----------(3)}$$

From equations (2) and (3),

$$A_o\eta_o = A_1\eta_1 + A_2\eta_2 \quad \text{----------(4)}$$

Consider one disintegration of the parent giving $\frac{C.\lambda_2}{\lambda_2-\lambda_1}$ disintegrations of the daughter, where C is a branching ratio constant. Then by equation (4)

$$\eta_o\left(1 + \frac{C.\lambda_2}{\lambda_2-\lambda_1}\right) = \eta_1 + \frac{C.\lambda_2}{\lambda_2-\lambda_1}.\eta_2 \quad \text{---------(5)}$$

and

$$Io = Ao\eta o = A_1\eta_1 + \frac{A_1\, C\cdot\lambda_2}{\lambda_2-\lambda_1}\cdot\eta_2$$

ie $$A_1 = \frac{Io}{\eta_1 + \frac{C\ \lambda_2}{\lambda_2-\lambda_1}\eta_2} \qquad \text{----------(6)}$$

This is the solution required for the first case.

Substituting $\eta o\left(1 + \frac{C\cdot\lambda_2}{\lambda_2-\lambda_1}\right)$ for $\eta_1 + \frac{C\cdot\lambda_2}{\lambda_2-\lambda_1}\cdot\eta_2$

(by equation (5)) into equation (6) gives,

$$A_1 = \frac{Io}{\eta o\left(1 + \frac{C\ \lambda_2}{\lambda_2-\lambda_1}\right)} \qquad \text{----------(7)}$$

This is the solution required for the second case. Equation (7) was used only in the case of antimony-129, for which it was necessary to measure the counter efficiency of the Sb^{129}/Te^{129} mixture directly, as the beta-spectrum of Sb^{129} was not sufficiently well known to allow the estimation of η_1.

Chapter 3

Mass-yield Measurements

a) Introduction

The method of mounting the sources, the electronic equipment employed and the counter calibrations were discussed in chapter 2. The isotopes on which the measurements were based are now considered and the chemical separations outlined. A list of these isotopes is given in table 3.1.

Fission-product activities from irradiations were not sufficient to permit aliquots of the active material to be taken and one isotope separated from each. Instead, the carriers for the reference isotope, in nearly all cases about 10mg. each, were added to the total active material - uranyl nitrate plus fission-products - in solution.

A rough chemical separation of each isotope was made and the crude fractions then purified by published radiochemical methods which however sometimes required

Table 3.1 A list of the isotopes separated

Mass no.	half-life	nuclide isolated
91	9.67 hr	Sr^{91}
93	10.15 hr	Y^{93}
Ref. 99	66.70 hr	Mo^{99}
105	4.44 hr	Ru^{105}
107	21 m	Rh^{107}
129	4.41 hr	Sb^{129}
131	8 d	I^{131}
143	33.40 hr	Ce^{143}
145	5.96 hr	Pr^{145}

modification. Most of the elements gave rise to precipitates of known composition; these could be weighed and the chemical yield of the separation thus obtained gravimetrically. The rare-earths, praesdymium, cerium and also yttrium, had no such convenient weighing form. They were determined by titration against standard ethylendiamine tetraacetic acid (EDTA) solutions after completion of the counting. Ruthenium also had no precipitate suitable for gravimetric use: the dioxide used in making the sources was determined spectrophotometrically. These supplementary chemical methods are described later where appropriate for each element.

The chemical methods of separation for each element are given in detail in the appendix.

The decay chains quoted for each mass were all taken from the review by Herrmann[3.1]. The half-lives used in the least-squares decay curve calculations in chapter 3 were also those from this review.

Self-absorbtion curves for each isotope separated in this work are given in figures 3.2, 3.3, 3.4. The

curves were constructed as described in chapter 2; all corrections for daughter activities have been applied.

b) The Reference Element

The choice of reference element required that it have an isotope produced in high yield with an easily resolvable decay and that the separation chemistry should be capable of routine, fairly simple application to give products of good purity. A further requirement is that it has a separation chemistry interfering little with other elements to be separated.

The first choice of reference element was zirconium -97. Its standard separation chemistry[3.2] was found capable of giving a pure radiochemical product and the first step, a precipitation with mandelic acid from 1 molar acid solutions did not interfere with the chemistry of the other elements. The isotope has a convenient half-life of 17 hours and the daughter, 74 minute Nb^{97}, is in transient equilibrium after about six hours thus adding to the activity of the sources.

A series of determinations made early in the course of

yield measurements on Sr^{91}, Y^{93} and Mo^{99} gave scattered results using Zr^{97} as the reference and it was concluded that complete isotopic exchange had not taken place between zirconium produced in fission and its isotopic carrier. It is well known that zirconium readily forms oxygen-bridged polymeric species in solutions of less than 1 molar acid. Pilkington & Wilson[3.3] have shown that once polymerised, zirconium does not split into mono-nuclear species unless refluxed with sulphuric acid greater than 5 normal.

Because of the doubts raised concerning the behaviour of zirconium during the redox steps designed to ensure isotopic exchange of all elements whose carriers had been added, it was decided to use Mo^{99} as a reference instead.

Mo^{99} has a longer half-life (66.7 hrs) than Zr^{97}. The Tc^{99m} daughter is in transient equilibrium and allowance must be made for its contribution to the measured activity.

Molybdenum-99 has the further advantage of being the reference isotope in the collection of fission-yields for U^{238} excited by fission-spectrum and 14 MeV neutrons by

Walker, Bonyushkin and Petrzhak[3.4, 3.5, 3.6]. This makes the comparison of the results of this work with those of previous workers more direct.

With the development of the computer programs as outlined in chapter 4, the counting of molybdenum became simplified. About eight counts taken over three or four half-lives were usually sufficient to define the molybdenum Ao activity with a standard deviation of 1%.

c) The Determinations of the Individual Isotopes

Strontium-91

The decay chain of mass 91 is

$$8.4s\ Kr \longrightarrow 71s.\ Rb \longrightarrow 9.67hr\ Sr \begin{cases} 59\% \rightarrow \text{st. Zr} \\ \rightarrow 58.9d\ Y \rightarrow \text{st. Zr} \end{cases} \quad 50m$$

Sr^{92} has a 2.68hr half-life and Y^{92} one of 3.52hrs. The strontium separation and purification was therefore carried out and the strontium left for 26 hours to allow Sr^{92} to decay completely. A convenient and rapid separation of Y^{92} which remained with the strontium carrier was obtained by first extracting the strontium and yttrium from a hydrochloric acid solution at pH 4-5 into a 0.1 M[illegible] solution

of di (2 - ethyl hexyl) phosphoric acid (HDEHP) in petroleum ether then back-extracting the strontium into 0.1 M hydrochloric acid, leaving the yttrium in the organic phase.

The best separation of strontium from the bulk uranyl nitrate and fission-products was found to be by precipitation as the nitrate from fuming nitric acid. Carbonate precipitations from solutions containing gram amounts of uranium were found to be uncertain and to give low chemical recoveries. Further purification steps included reprecipitation as the nitrate and two scavenging steps with barium chromate. Strontium was finally precipitated as the carbonate, mounted and weighed to determine the chemical yield.

The use of nitric acid in the first separation step meant that the strontium separations were incompatible with certain other elements, notably ruthenium and rhodium. In practise, strontium was usually combined with the rare-earth or cerium separations. Molybdenum was recovered from the nitric acid solution by gently evaporating off the bulk of the acid and diluting before proceding further with the molybdenum method.

The strontium decay in nearly all cases could be analysed using a single component least-squares program; the main contaminant observed was Sr^{89} (50.4d) which together with Y^{91} (59d) constituted an essentially constant background throughout the decay period of strontium-91.

Self-absorbtion curves for Sr^{91} and the Y^{91m} daughter were constructed using the Bayhurst and Prestwood type curves discussed in chapter 2 and are shown in figure 3.2.

Yttrium-93

The decay chain of mass 93 is

$$1.2s\ Kr \longrightarrow 5.6s\ Rb \longrightarrow 7.54m\ Sr \longrightarrow 10.15hr\ Y \longrightarrow 9.5 \times 10^5 y\ Zr \longrightarrow \text{st. Nb}$$

The fission solution was left for 1½ hours before carrying out any chemistry upon it. Counting was not begun until some 35 hours had passed to allow the 3.5hr Y^{92} to decay away.

It was found that yttrium could be purified by processing it along with praesodymium on a cation exchange column. The details are given more fully in the section on praesodymium.

Gradient Elution Apparatus

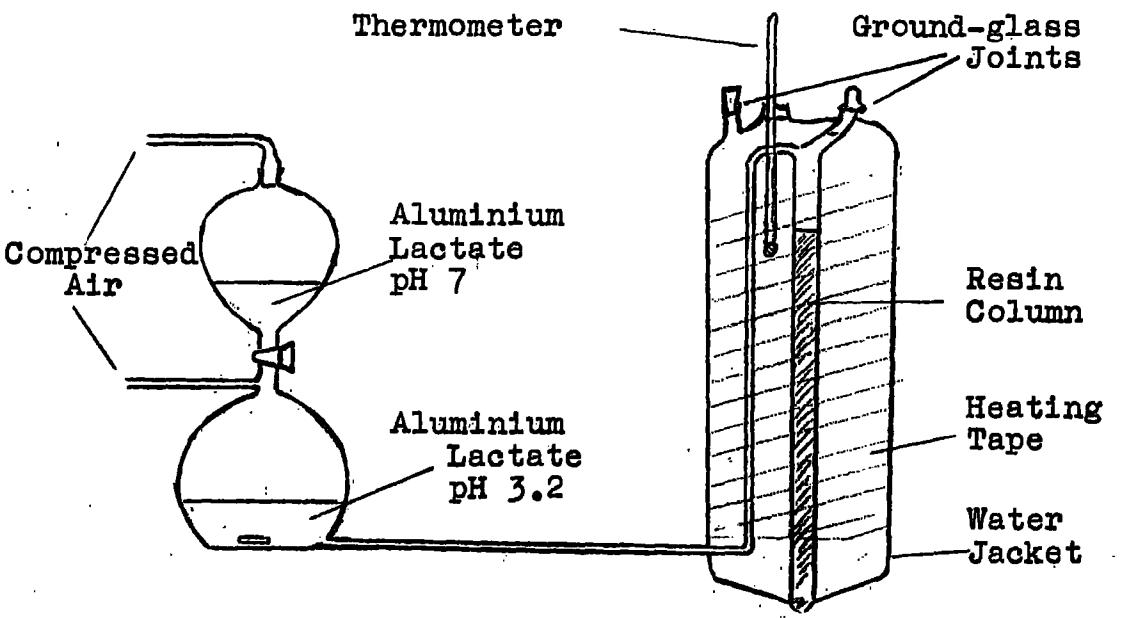

Figure 3.1

Briefly, the rare-earths were separated and purified as a group by repeated fluoride precipitations or by extraction into a 1 M solution of HDEHP in petroleum ether from 0.1 M hydrochloric acid and then back-extraction into a little concentrated hydrochloric acid. Actinides were removed by passing this acid phase through a small, strongly basic anion-exchange column and cerium was removed by extracting Ce IV with HDEHP in petroleum ether from 8 M nitric acid. Finally the lanthanides were adsorbed on the top of a cation-exchange column in the ammonium form and they were selectively eluted by gradient elution with 1 molar ammonium lactate solution.

Yttrium came off the column with the first of the rare-earths occurring in fission and it was precipitated and mounted as the oxalate before praesodymium was eluted.

The decay curves recorded for Y^{93} separated on the cation-exchange column showed a marked improvement over the decay curves of yttrium separated in early runs by extraction into tri n-butyl phosphate solutions in petroleum ether from 14 M nitric acid[3.7]. A single component least-squares

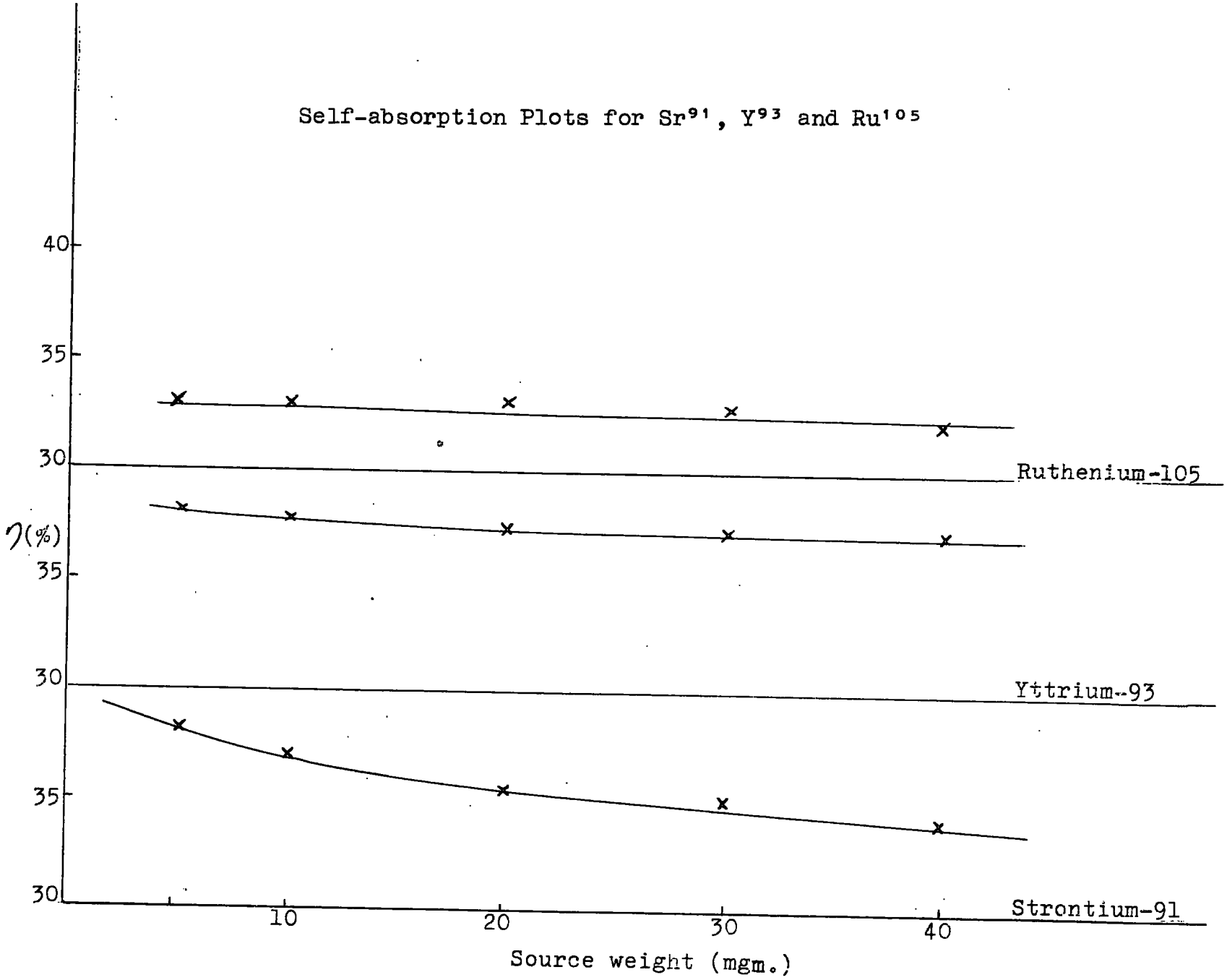
Self-absorption Plots for Sr91, Y93 and Ru105
40
35
30
η(%)
35
30
35
30
Ruthenium-105
Yttrium-93
Strontium-91
10
20
30
40
Source weight (mgm.)

Figure 3.2

program was found quite adequate to separate the activity of Y^{93} from long-lived yttrium activity.

Rare-earth oxalates are non-stochiometric and the radioactive sources were dissolved in dilute hydrochloric acid and determined by titration against a standard EDTA solution.

Direct titrations of lanthanides by EDTA was not possible in the presence of oxalate ions and to overcome this, for example, back-titrations employing Eriochrome Black T indicator have been used[3.8]. Walczynska[3.9] determined cerium oxalate by direct titration with EDTA after decomposing the precipitate with ammonium persulphate solution. The reaction is shown to be complete by the appearance of the Ce IV colour. This aid was not possible for yttrium or praesodymium but by using the same amounts of ammonium persulphate the titration was found to give clean end-points showing that all oxalate had been decomposed by the procedure.

Use of a direct titration method meant that Xylenol Orange could be utilised as indicator at pH 5.8-6.0.

This indicator gave very sharp end-points with lanthanides and the same titration was used for the carrier solutions enabling a direct comparison to be made of titration values for the chemical yields.

The self-absorbtion curve (fig.3.2) for Y^{93} was constructed from the standard Bayhurst-Prestwood type plots.

Molybdenum-99

The decay chain for mass 99 is

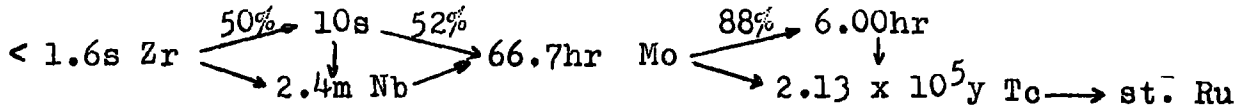

Mo^{99} had been chosen as the reference element for reasons discussed earlier. The classical radiochemical procedure of Ballou[3.10] is quite lengthy and has the experimental disadvantage of requiring a wet oxidation step.

Maeck, Kussy and Rein[3.11] gave a method for molybdenum which was found to be suitable, giving high purity molybdenum quickly and easily. The α-benzoin oxime precipitate of molybdenum, formed preferably from 1 M hydrochloric acid was extracted into ethyl acetate, washed several times with 1 M hydrochloric acid and back-extracted into 4 M

ammonia solution. The extraction steps were repeated, an ion scavenge performed and after adjusting the pH, molybdenum was precipitated as the 8-hydroyquinolate.

Observations showed that the α-benzoin oxime precipitate itself was extracted and it could in fact be extracted whenever the experimental conditions allowed the precipitate to be formed. From nitric acid solutions, uranium partially extracted into the ethyl acetate phase but this interference was eliminated by washing the extract with dilute hydrochloric acid.

The extraction of molybdenum was conveniently carried out first as it caused no interference with other carriers in the solution; excess α-benzoin oxine was removed with the ethyl acetate phase. Strontium was precipitated first however before the molybdenum extraction as explained earlier; rhodium was also precipitated first from solution because of the short half-life of Rh^{107} when it was made the basis of a yield measurement.

Self-absorbtion plots (fig. 3.3) for Mo^{99} and the daughter in transient equilibrium, Tc^{99m}, were constructed from Bayhurst and Prestwood type curves.

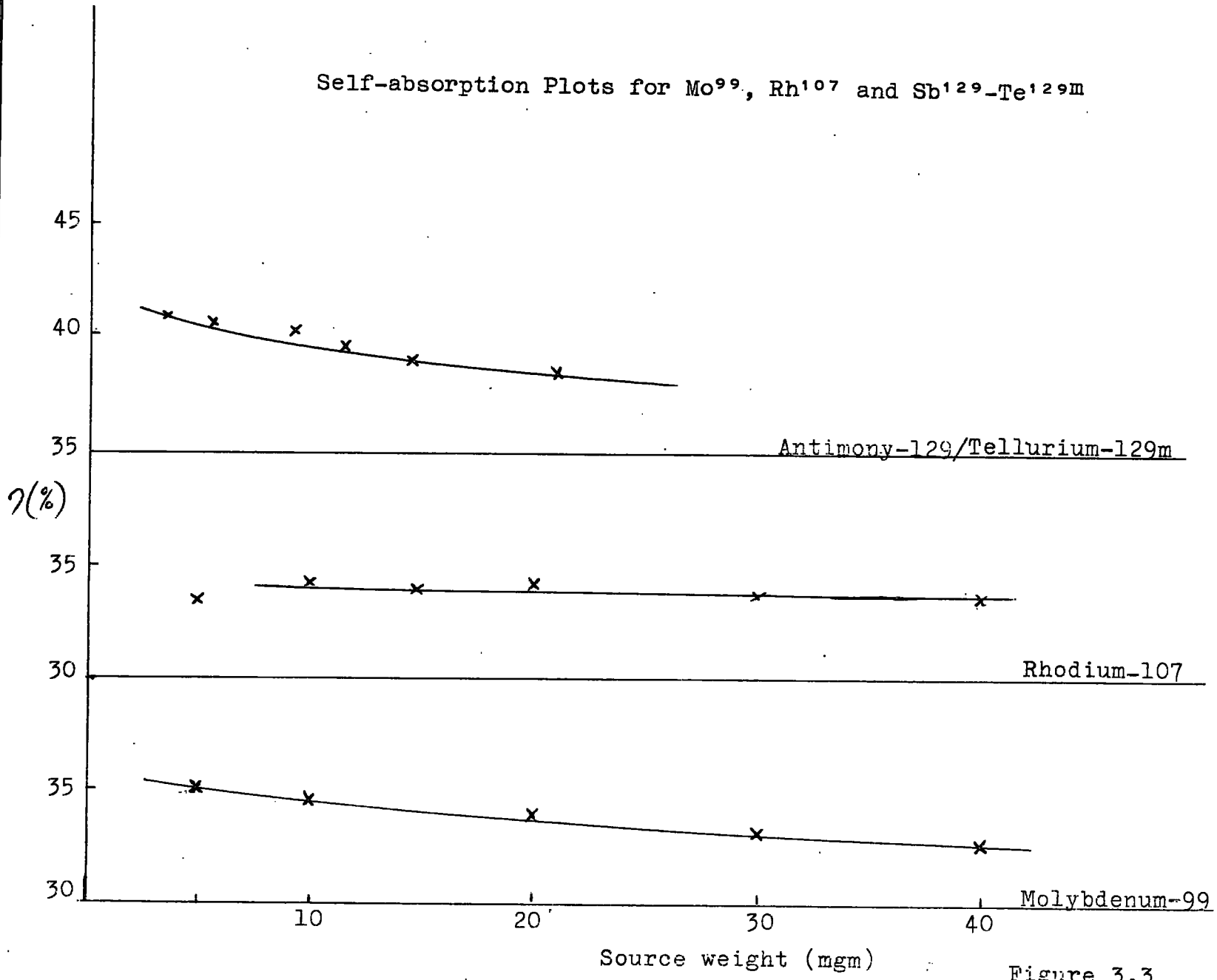
Self-absorption Plots for Mo99, Rh107 and Sb129-Te129m
45
40
35
η(%)
Antimony-129/Tellurium-129m
35
30
Rhodium-107
35
30
Molybdenum-99
10
20
30
40
Source weight (mgm)

Figure 3.3

Ruthenium-105

The mass-chain is

$$40s\ Mo \longrightarrow 7.7m\ Tc \longrightarrow 4.44hr\ Ru \xrightarrow{25\%} 36hr\ Rh \longrightarrow st$$
$$\qquad\qquad\qquad\qquad\qquad\qquad\qquad\qquad\qquad\qquad\qquad\qquad \searrow 45s$$

The irradiated sample was left for 1.5 hours before any chemistry was attempted. Ruthenium has several valency states and therefore to ensure isotopic exchange between fission-product and carrier ruthenium, the solution was boiled for 10 minutes with 2 drops of bromine and reduced with hydroxylamine after cooling. Ruthenium was precipitated as Ru_2S_3 by passing H_2S through the solution; the solid was slurried into a distillation apparatus with dilute sulphuric acid. 'Sodium bismuthate' was added and ruthenium (VIII) oxide was distilled into ice-cold 12 molar sodium hydroxide solution. After a ferric hydroxide scavenge step, ruthenium dioxide was precipitated from acid solution by the addition of ethanol.

Very poor yields were obtained from irradiations with 3 MeV neutrons. It was thought that the nitrate from the ten grams of uranyl nitrate irradiated in this work might have caused some ruthenium to extract with molybdenum into ethyl acetate and therefore irradiations were carried

out using about six grams of uranium trioxide instead. Appreciably better yields were recorded thereafter.

Self-absorbtion curves for Ru^{105} and Rh^{105m} (fig. 3.2) were constructed from curves of the Bayhurst and Prestwood type.

The daughter product Rh^{105} undergoes appreciable decay during several half-lives of ruthenium. It is shown in more detail in chapter 4 that a parent daughter relation of the type including ruthenium and rhodium-105 can be represented by a two component decay equation,

$$A = A_1^o e^{-\lambda_1 t} + A_2^o e^{-\lambda_2 t} + c$$

where c represents an activity very long lived relative to the ruthenium. The equation was solved for the parameters A_1^o, A_2^o and c by the method of least-squares using the two-component computer program of chapter 4.

Rhodium-107

The mass-chain 107 is

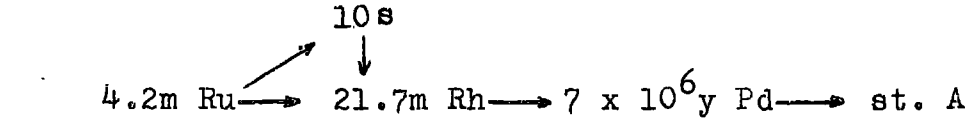

The 21.7 minute rhodium isotope is a very useful one

for mass-yield measurements, lying on the heavy side of the light peak where isotopes convenient for experimental yield measurement are rare. The chemistry of rhodium however is notoriously difficult as most of the complexes formed in aqueous solution are kinetically inert. The only complex suitable for solvent extraction on the milligram scale which has been used in radiochemical separations is that formed with pyridine[3.12]. Other extractable complexes such as that formed with mercaptobenzoxazole are exceedingly difficult to break down to allow back-extraction of rhodium.

The method favoured by Chenley, Osmond and Perry[3.13] is that of precipitation as $K_3Rh(No_2)_6$. Nitrite complexes of rhodium are readily formed in aqueous solution and they are stable in neutral or alkaline solutions but decompose when warmed with dilute acid.

It was found possible to use this method for the 14 MeV irradiations but for the 3 MeV irradiations, the increase in the amount of uranium irradiated, meant that very poor chemical yields were recorded. Even for the 14 MeV runs only about half of them were successful. The main trouble was that the potassium hexanitritorhodate(III) did not

precipitate until the pH of the solution was fairly high. Uranium(VI) oxide contamination was often heavy and on occasions a precipitate insoluble in acids on boiling and presumed to be a hydrated rhodium oxide was formed.

A gravimetric method for the determination of rhodium as the hexammino-cobalt(III) hexanitrito-rhodium(III) salt, quoted by Beamish[3.14] was found to be very useful in producing a weighing form for rhodium suitable for making sources. Since the hexanitrito-rhodate anion appears to give insoluble salts with large cations (K^+, $(NH_3)_6\ Co^{3+}$), it was thought possible that a substitute for potassium might be found for use in radiochemical separations. Caesium and thallium(I) ions were both found to precipitate rhodium from nitrite solutions. Thallium was selected because it could easily be removed from solution as thallium(III) oxide after oxidation. This precipitation also acted as a scavenging step in the method devised.

The solution of fission-products and uranyl nitrate with 10 mg. of rhodium as hexachlororhodate(III) in one molar hydrochloric acid was boiled and bromine added to help promote isotopic exchange: this part of the procedure

was started 35 minutes after the end of the irradiation. A saturated solution of sodium nitrite was added to neutralise the solution which was kept warm for 5 minutes to ensure that all the rhodium was present as the nitrite complex, $Rh(NO_2)_6^{3-}$. The thallium complex was precipitated by the addition of thallium(I) nitrate. The precipitate was dissolved in aqua regia, rhodium complexed with sodium nitrite and thallium precipitated by making the solution alkaline with sodium hydroxide. The final precipitate of $Co(NH_3)_6$ $Rh(NO_2)_6$ was brought down by adding a saturated solution of hexammino-cobalt(III) chloride to the warm slightly acid nitrite solution.

The rhodium carrier solutions were standardised as specified by Beamish[3.14] by precipitation as $Co(NH_3)_6$ $Rh(NO_2)_6$ and as a check, by igniting to the metal from a sulphide precipitation.

Self-absorbtion plots for Rh^{107} (fig. 3.3) were prepared from curves of the Bayhurst-Prestwood type.

The above procedure gave activity that resolved very cleanly into 21.7m Rh^{107} and 36hr Rh^{105}. No other radioactive isotope was observed during decay down to background

level. The ratio of the rhodium half-lives - a factor of approximately 100 - meant that a single component least-squares treatment was quite sufficient to give accurate A^{o} values for Rh^{107}. The separation procedure took between 30 and 40 minutes each time. Together with the 35 minute waiting period for Ru^{107} to decay, four complete rhodium half-lives were usually lost before counting could be started.

Antimony-129

The 129 mass-chain is

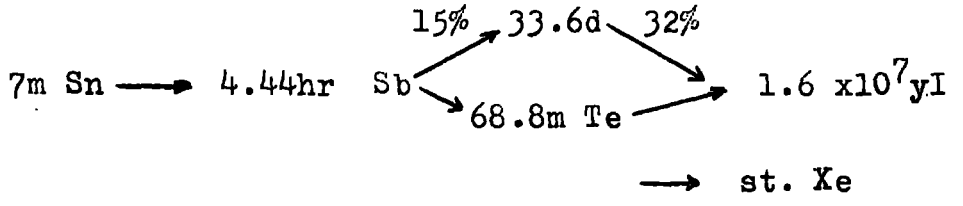

Antimony was separated by precipitation as sulphide from the fission-product solution after a redox step with bromine and hydroxylamine. The sulphide was dissolved in concentrated hydrochloric acid and a tellurium metal scavenge performed on the solution. The last two steps were repeated and antimony was finally purified by extraction as antimony(V) into di-isopropyl ether followed by a back-extraction as antimony(III) into dilute hydrochloric acid.

The final precipitation of antimony has proved difficult in the past: sulphide precipitation, by passing hydrogen sulphide gas results in a non-stochiometric precipitate which has to be analysed later for antimony and precipitation as the n-propyl gallate requires time for appreciable precipitation to take place.

Morandat and Duval[3.15] have recommended the precipitation of antimony as sulphide by digesting an acid solution of antimony(III) in the presence of excess ammonium thiocyanate and the method was adopted for this work. It is a homogeneous precipitation method and gave fine granular precipitates of Sb_2S_3 of a distinctly darker red colour than that obtained from H_2S precipitation, indicating the comparative absence of free sulphur in the sources.

The carrier antimony solution was standardised using this method and the result so obtained agreed within 0.5% with determinations made using n-propyl gallate.

Counter efficiences could not be determined using the Bayhurst-Prestwood type curves as there were not sufficient data available on the beta-spectrum of Sb^{129}. Moreover,

previous counter efficiency determinations made by other workers from this laboratory gave unusually high values for similar types of counters after allowing for the tellurium-129 daughter which is in transient equilibrium[3.16].

The counter efficiency for antimony-129 was therefore determined by preparing a highly active sample of antimony-129 separated from ten grams of uranyl nitrate irradiated for an hour with 14 MeV neutrons. Less than 1 mg of carrier was used and the resultant antimony sulphide precipitate was dissolved in hydrochloric acid. The activity of this solution was determined by $4\pi-\beta-$ proportional counting as described in chapter 2. A known amount of antimony carrier was mixed with the active solution and sources made. The self-absorbtion plot (fig. 3.3) was made in a similar way to the standard Bayhurst-Prestwood plots.

The counter efficiency found for the antimony tellurium-129 pair was 40% for a 10 mg source. The efficiency for tellurium-129 from the Bayhurst-Prestwood plots was measured at 34% at this source weight. From equation 5 in chapter 2 the efficiency of antimony-129 was

found to be 46.6% by calculation.

The reason for this high efficiency, which does not lie on the Bayhurst-Prestwood type curves is not known. Independent corroboration of the value obtained is given by values of counter efficiences measured for similar counters on this isotope[3.17].

94hr antimony-127 was always present and observed in the antimony decay curves. A two-component least-squares program was employed to sort out the data. Standard deviations of 2% were obtained for the A^{o} value for antimony-129 using this program.

Iodine-131

The decay-chain for mass 131 is

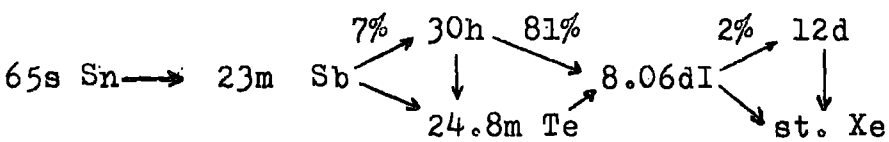

The irradiated sample was left for ten days before any chemistry was started to allow the long-lived precursors of iodine-131 to decay.

Iodine was separated from samples of uranyl nitrate

irradiated by 14 MeV neutrons using the method given by Meinke[3.18]. The sample was dissolved in dilute hydrochloric acid and 10mg of iodine and molybdenum carriers were added. The solution was made alkaline and the uranium was held in it with sodium carbonate. Warming with sodium hypochlorite oxidised the iodide to periodate and after acidification and reduction with hydroxylamine hydrochloride solution, elemental iodine was extracted into carbon tetrachloride.

Iodine was reduced to iodide with sulphur dioxide and a final purification cycle consisting of an oxidation to iodine with nitrite, and a carbon tetrachloride extraction step as before was carried out. Palladium(II) iodide was finally precipitated and mounted for counting.

The weight of the source gave the yield of iodine when compared to the gravimetric determination of iodide in the carrier as palladium(II) iodide[3.19].

With 10gm of uranyl nitrate to analyse in the irradiations with 3 MeV neutrons, the acidification of an alkaline solution was found to be difficult to control as excessive amounts of carbon dioxide were produced. Initial iodine

chemical yields were low for the 3 MeV determinations, possibly due to iodine being volatilised or otherwise carried out of the system at this stage.

A method given by Marsh in a series of radiochemical separation procedures published by the University of California[3.20] was therefore employed. Following this method, all iodine was oxidised by sodium chlorate to iodine monochloride from 6 M hydrochloric acid solution. The iodine monochloride was extracted into butyl acetate, iodine was back extracted into water after reduction with sulphurous acid and as in the previously mentioned procedure of Meinke an oxidation-reduction extraction cycle was carried out. Good yields of palladium(II) iodide were obtained using this method and the decay curves did not show signs of contamination. The curves were analysed satisfactorily using a single component least-squares program.

As I^{131} was one of the isotopes employed to construct the Bayhurst-Prestwood type curves, the counter efficiency for this isotope was determined using the original I^{131} measurements. These are shown in figure 3.4.

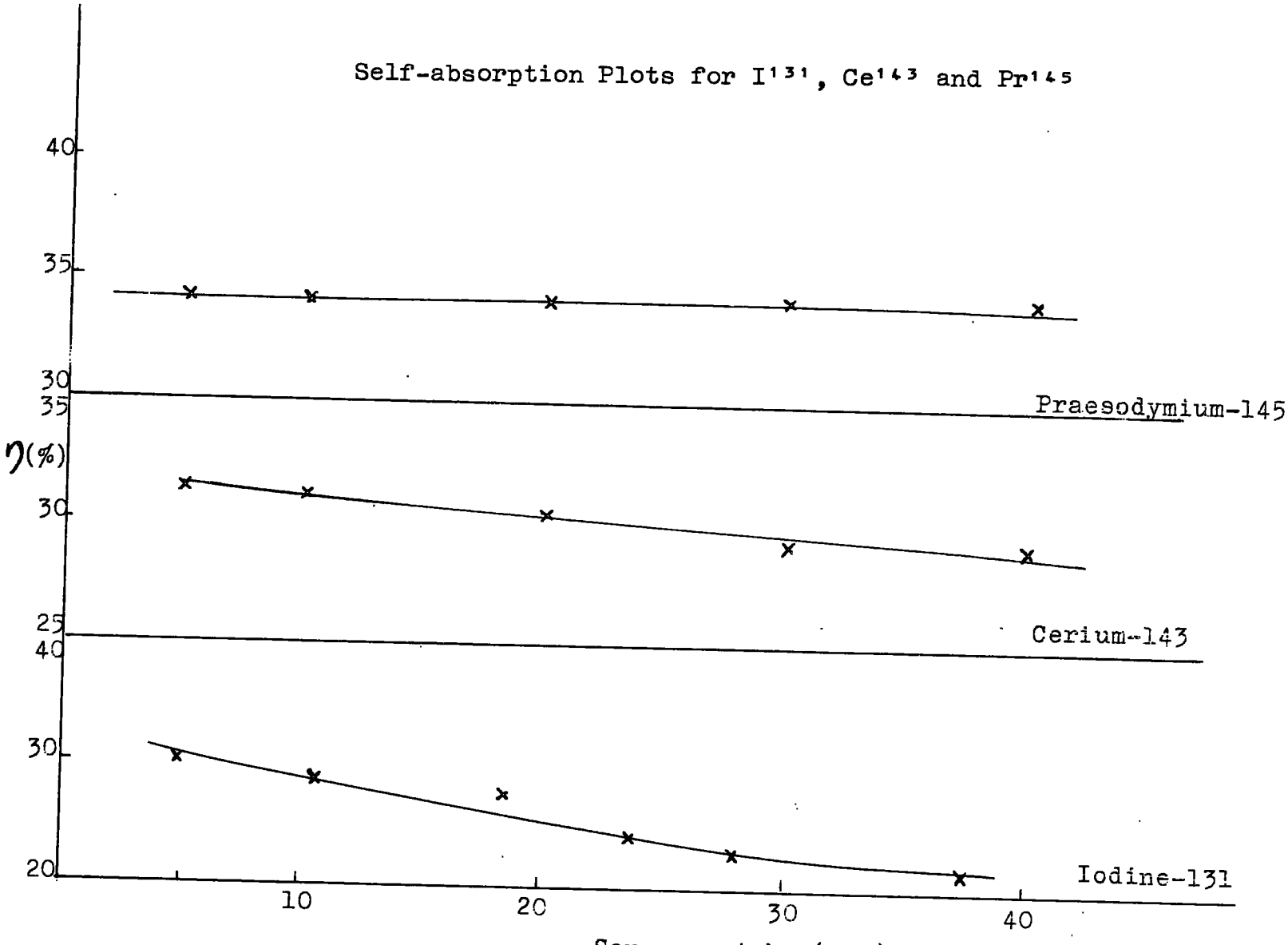
Self-absorption Plots for I^{131}, Ce^{143} and Pr^{145}
40
35
30
35
Praesodymium-145
η(%)
30
25
40
Cerium-143
30
20
Iodine-131
10
20
30
40
Source weight (mgm)

Figure 3.4

Cerium-143

Cerium was chosen to determine the yield of the mass 143 chain

2s Cs ⟶ 12s Ba ⟶ 14m La ⟶ 33.4hr Ce ⟶ 13.59d Pr ⟶ st. Nd.

Cerium(III) has a chemistry typical of the lanthanides but the well-defined cerium(IV) oxidation state provides a means for the separation of cerium from other rare-earths. Such separations have been made by for example, selective precipitations of cerium(IV) iodate from acid solution or extraction of cerium(IV) from 10 M nitric acid solution into methyl isobutyl ketone[3.21].

Di (2-ethylhexyl) orthophosphoric acid (HDEHP), has been shown to have a high extraction coefficient for cerium(IV) with respect to trivalent lanthanides from nitric acid solutions[3.22]. The method used in this work was based on such a separation given in the University of California procedures[3.20].

A waiting period of three hours was necessary following

the irradiation to let the 14m La^{143} precursor decay. Isotopic exchange was ensured by redoxing fission-products and carrier in acid solution with bromine and hydroxylamine. Cerium was separated with the rare-earths by repeated precipitations with fluoride. Three extractions with 0.1 M HDEHP in carbon tetrachloride were made upon the rare-earths in 4 M nitric acid to eliminate tetravalent ions, zirconium and thorium. The rare-earths were again precipitated with ammonium-hydroxide, cerium oxidised to Ce(IV) with potassium bromate and extracted into 0.3 M HDEHP in petroleum ether from 4 M nitric acid. Cerium(III) was back-extracted by shaking the organic phase with 0.5 M nitric acid plus two drops of hydrogen peroxide solution. An additional scrub with 6 M hydrochloric acid and a little hydroxylamine was usually incorporated to completely back-extract the cerium. Cerium(III) was finally precipitated as the oxalate; the source was washed with ethanol and ether and dried under a vacuum.

The University of California procedure calls for an adsorbtion of cerium on a small cation-exchange column (Zeocarb 225, 8% D.V.B., 100-200 mesh, sodium form was used)

and subsequent elution with ammonium lactate solution (1 molar, pH 7.0) at the stage immediately preceding the final precipitation as oxalate. Sources of very high weight were obtained when this step was included and the interference was finally found to be due to calcium and magnesium eluted from the resin. Unsatisfactory end-points were found in the EDTA determinations of these sources and they were therefore determined colorimetrically, measuring the absorbtion due to cerium(IV) after oxidation with potassium persulphate[3.23]. Cerium sources obtained without including the small cation column stage were determined by destroying the oxalate with ammonium persulphate and titrating the cerium with 0.01 M EDTA solution at pH 5.8 using Xylenol Orange as an indicator[3.9].

Counter efficiency curves for Ce^{143} (fig. 3.4) were constructed using the curves of the Bayhurst-Prestwood type.

Both Ce^{141} (32.5d) and the Ce^{143} daughter, 13.59d Pr^{143} were unavoidably present in the samples counted. The decay curves could be resolved using a two-component

least-squares program by treating the long-lived activity as a single component with a half-life of 26 days. This was possible without introducing appreciable errors into the Ce^{143} activity determined because the Ao value of the short half-life component was found to be insensitive to the exact value chosen for the decay constant of the second component.

Praesodymium-145

The decay chain for mass 145 is

3.0m Ce ⟶ 5.96hr Pr ⟶ st. Nd.

At least 30 minutes were allowed for Ce^{145} to decay before the separation procedure was started. Praesodymium was isolated in a group separation as outlined above for cerium and yttrium. A quicker alternative for the group purification was found to be to extract the rare-earths into 0.3 M HDEHP in petroleum ether from 0.1 M hydrochloric acid solution. When 10gm of uranyl nitrate were irradiated, a first separation by fluoride precipitation was necessary but when only two or three grams were irradiated an initial separation of the rare-earths by

precipitation as hydroxides from a carbonate solution was more convenient.

After extraction into 0.3 M HDEHP and thorough washing with 0.1 M hydrochloric acid the lanthanides were back-extracted into three millilitres of 10 M hydrochloric acid. The acid phase was passed through a small strongly basic anion column (Deacidite FF in the chloride form) to adsorb traces of actinides.

The individual separations of the rare-earths were performed by a gradient elution from a cation exchange column using ammonium lactate-lactic acid[3.24].

The column, 60 x 0.7cm, was surrounded by a water-jacket to permit operation at 90°C (fig. 3.1). The resin was Bio Rad AG Dowex 50, 400 mesh, 4% D.V.B. in the ammonium form. The resin had previously been washed with ammonium thiocyanate, dilute hydrochloric acid and distilled water and converted to the ammonium form by washing with 1 M ammonium lactate solution at pH 7.

Up to 20 mg of the rare-earth carriers in total were adsorbed on the column by digesting a very weakly acid

solution with 1 ml of the resin which was then placed on the column with a pipette and allowed to settle.

A lactic acid solution was made by refluxing A.R. lactic acid with 0.1 M hydrochloric acid to destroy any anhydrides present and then diluting the mixture to give a 1 M solution. Solutions having a pH of 3.2 and 7.0 were prepared by adjusting the pH of the lactic acid solution with concentrated aqueous ammonia.

To elute the rare-earths, ammonium lactate solution at pH 3.2 was passed through the column for an hour at the rate of 4 drops per minute. Ammonium lactate of pH 7.0 was then allowed to mix with this solution at a rate of 8 drops per minute, the mixed flow rate through the column meanwhile being held constant. Starting with 100 ml of lactate at pH 3.2 and 60 ml of pH 7.0, praesodymium was eluted from the column in about 8 hours under the above conditions.

An automatic fraction collecting apparatus was controlled by a photo-electric device which counted every drop eluted from the column and changed the fraction every 30 drops.

Chapter Four

The Analysis of Decay Data by Computer Methods

Of the measurements required for the calculation of relative yields, those which contribute the most error may be considered to be the activity at the end of the irradiation (Ao) and the counter efficiency (η). In this work the counter efficiencies were determined by utilising the method of Bayhurst and Prestwood for counter calibration as discussed in chapter 2. A description is given in this chapter of a method for the analysis of decay data used to minimise errors in Ao values.

Ao determinations are regularly made in radiochemical work by plotting on semi-logarithmic graph paper the measured activity against the time which has elapsed since the end of the irradiation. This well-known method can be faulted in several aspects. The lack of sensitivity to the half-life value used in drawing a straight line through the points is quite marked and this difficulty in constructing the straight line can be aggravated by the abnormal effective weighting attached to the low activity points by the semi- logarithmic plot. The question of the weighting of

points is discussed below.

With two-component samples, the same plot gives a curve which with increasing time straightens into a line of slope determined by the half-life of the longer-lived activity. The Ao values are then determined by extrapolating the longer-lived activity back to zero time and subtracting it from the total activity curve to leave a straight line having the half-life of the shorter-lived component. This curve-stripping process is tested in practice by observing the fit of the points left after stripping to a straight line with the slope expected from the half-life of the short-lived component. However it can be observed, in practice, that quite wide variations in the position of the line drawn through the long-lived points can give passable straight lines for the short lived component.

Estimates for the Ao value of the short-lived activity found by curve stripping when compared with least-squares results at the beginning of this work were invariably found to be low by a few percent, showing that the tendency in stripping semi-logarithmic plots had been to subtract too

much activity.

One apparent solution would be to measure only those isotopes which on separation from fission-products give straight-line decay curves on semi-logarithmic paper. However such cases impose severe restraints on the half-lives of other isotopes of the separated elements and on associated daughter activities which are inevitably counted as well.

This restricting policy in any case, does not allow values of the errors of the parameters to be determined. There is therefore no objective criterion of goodness of fit which can be applied to the graphical method of analysis. A least-squares determination of the decay-curve parameters is attractive in that it can meet the three main objections to the graphical method: firstly an objective evaluation of the parameters, secondly a reliable weighting procedure and thirdly calculations of the errors of the parameters are all feasible.

The general problem in the analysis of decay data is the determination of the parameters Aio and λi in the

equation

$$A_t = \sum_{i=1}^{N} Aio\ e^{-\lambda i.t} \quad \text{.....(1)}$$

where A_t is the observed activity at time t. Aio and λi are the zero-activity and decay constant of each of the component activities.

The problem in this work had a simpler form. The decay constant were assumed to be best literature values and the number of component activities was limited to two. The case having the greatest number of components was that of

$$A_t = A_{1o}\ e^{-\lambda_1 t} + A_{2o}\ e^{-\lambda_2 t} + C \quad \text{.....(2)}$$

where C is here the contributions due to relatively very long-lived activities which could be considered not to change during the period of counting and which may include the background. Three parameters were determined in this case: A_{1o}, A_{2o} and C.

Two more cases were also found to be useful for application to different types of decay systems. Firstly the single-component decay having a long-lived background:

$$A_t = A_{1o}\ e^{-\lambda_1 t} + C \quad \text{.....(3)},$$

and an adaptation of the example given in equation (2) for use with long-lived contaminations having mixed or more indeterminate half-lives:

$$At = A_{1o}\, e^{-\lambda_1 t} + A_{2o}\, e^{-\lambda_2 t} \quad \text{.....(4).}$$

The parameters to be determined in equation (3) are A_{1o} and C and those in equation (4), A_{1o}, A_{2o} and λ_2.

Ruthenium-105 and antimony-129, both of which have daughters with half-lives sufficient to prevent the application of equation (3) could be treated using equations (2) or (4) as can be seen by the following argument:

A mixture of parent-daughter activities can be described by the equation

$$A_t = A_{po}\, e^{-\lambda_p t} + A_{do}\, e^{-\lambda_d t} + A_{po}\left(\frac{\eta_d}{\eta_p}\right)\left(\frac{\lambda_d}{\lambda_d-\lambda_p}\right)\left(e^{-\lambda_p t} - e^{-\lambda_d t}\right)$$

where the subscripts 'p' and 'd' represent the parent and daughter activities.

Rearranging terms and putting $A_{do} = o$,

$$At = A_{po}\, e^{-\lambda_p t}\left(1+\left(\frac{\eta_d}{\eta_p}\right)\left(\frac{\lambda_d}{\lambda_d-\lambda_p}\right)\right) - e^{-\lambda_d t}\left(\frac{\eta_d}{\eta_p}\right)\left(\frac{\lambda_d}{\lambda_d-\lambda_p}\right)$$

if this equation is fitted by least-squares analysis to

$$At = A_{1o}\, e^{-\lambda_1 t} + A_{2o}\, e^{-\lambda_2 t} + C$$

then

$$A_{1o} = A_{po}\left(1 + \left(\frac{\eta_d}{\eta_p}\right)\left(\frac{\lambda_d}{\lambda_d - \lambda_p}\right)\right)$$

$$A_{2o} = -\left(\frac{\eta_d}{\eta_p}\right)\left(\frac{\lambda_d}{\lambda_d - \lambda_p}\right)$$

and therefore $A_{po} = A_{1o} + A_{2o}$,

Least-squares programs for the analysis of counting data have been written[4.1, 4.2] but because of the lack of availability of these programs together with the fact that they appear to have been written in FORTRAN - a language which the computer available could not accept - and also because from their description, the programs looked too sophisticated for the problems in hand, it was decided to write programs for the cases defined by equations (2), (3) and (4).

Counting statistics are well-known to follow a Poisson distribution[4.3]. Least-squares regression techniques which are commonly employed in the statistical analysis of data are rigorously applicable to normally distributed observations. However normal distributions can be shown to

approximate Poisson distributions and therefore apply to counting statistics except when the count rate is low. An additional advantage is gained from being able to apply Poisson statistics in that the standard deviation of each observed count may be calculated from the total number of observed events in that count alone and not just the relation of that point to the whole distribution.

This property of decay data immediately allows a value to be assigned to the weight of each point. Since the weighting in least-squares analysis is defined as being inversely proportional to the variance it is therefore in the case at point, proportional to the reciprocal of the total number of counts recorded.

Wentworth[4.4] has written a paper showing the application of rigorous least-squares methods to data analysis. His treatment is taken from a book by Deming[4.6] and this in turn has been used as a primary reference in this work.

To show the application of Wentworth's treatment, the simplest decay structure scheme as given by equation (3) will be used as an example. The treatment was general

enough to allow ready extension to fit the other two cases.

Several distinct steps set out below were needed.

a) Estimates of the parameters had to be provided. They were generally obtained from a graphical analysis although the least-squares solutions were found to be quite insensitive to the estimated parameter values.

b) Writing equation (3) in the form

$$A_{1o}\, e^{-\lambda_1 t} + C - At = F \qquad \ldots\ldots\ldots\ldots\ldots\ldots (5)$$

the partial derivations with respect to the parameters, A_{io}, and C and the variables t and At were calculated.

$$FA_{1o} = e^{-\lambda_1 t} \qquad \ldots\ldots\ldots\ldots\ldots\ldots (6)$$

$$FC = 1 \qquad \ldots\ldots\ldots\ldots\ldots\ldots (7)$$

$$FAt = -1 \qquad \ldots\ldots\ldots\ldots\ldots\ldots (8)$$

$$Ft = -\lambda_1 A_{1o}\, e^{-\lambda_1 t} \qquad \ldots\ldots\ldots\ldots\ldots\ldots (9).$$

In this terminology, FA_{io} represents the partial derivative

$$\left(\frac{\partial F}{\partial A_{io}}\right)\Big/_{C,At,t} .$$

c) the partial derivatives in equations (6) to (9) were evaluated for each data point (Ai, ti) together with F^o_i where $F^o_i = A^o_{io}\, e^{-\lambda_1 t_i} + C^o - Ai$ .....(10). A^o_{io} and C^o are the estimated parameters.

The function Li was evaluated. This includes the partial derivations of the variables and the weights:

$$L = \frac{FA_t . FA_t}{WA_t} + \frac{F_t . F_t}{W_t} \quad \ldots\ldots\ldots\ldots\ldots\ldots (11)$$

The activity, A_t, is not a directly observed variable. If Mi is the total number of counts recorded and Δti the duration of that particular count then

$$Ati = \frac{Mi}{\Delta ti}$$

This gives L the form

$$L = \frac{F_M . F_M}{W_M} + \frac{F_t . F_t}{W_t} + \frac{F\Delta t . F\Delta t .}{W\,\Delta t}$$

t and Δt are assumed to be measured without error, i.e. they have infinite weight. W_M has the value of 1/variance(M) = 1/M and $F_M = {}^1/\Delta t$.

$$\therefore \quad Li = \frac{Mi}{(\Delta ti)^2} \quad \ldots\ldots\ldots\ldots\ldots\ldots\ldots\ldots\ldots\ldots\ldots (12).$$

d) The normal equations were constructed. In this example they were

$$\sum_{i=1}^{N} \frac{FA_1oi \,.\, FA_1oi}{Li} . \Delta A_{1o} + \sum \frac{FA_1oi \,.\, Fci}{Li} . \Delta c = \sum \frac{FA_1oi \,.\, Fi^o}{Li}$$

$$\sum \frac{FCi \,.\, FA_1oi}{Li} . \Delta A_{1o} + \sum \frac{FCi \,.\, FCi}{Li} . \Delta c = \sum \frac{FCi \,.\, Fi^o}{Li}$$

These equations were to be solved for ΔA_{1o} and ΔC.

If A_{1o} and C are the least-squares corrected estimates of the parameters

then

$$A_{1o} = A^{o}_{1o} - \Delta A_{1o} \quad \ldots\ldots\ldots\ldots\ldots\ldots\ldots\ldots(13)$$

$$C = C^{o} - \Delta C \quad \ldots\ldots\ldots\ldots\ldots\ldots\ldots\ldots(14)$$

A matrix-inversion solution was applied to the normal equations. If they are written as

$$b11.\Delta A_{1o} + b12.\Delta C = C1 \quad \ldots\ldots\ldots\ldots\ldots\ldots(15)$$

$$b21.\Delta A_{1o} + b22.\Delta C = C2 \quad \ldots\ldots\ldots\ldots\ldots\ldots(16)$$

then the solution is given by

$$\Delta A_{1o} = d11\ C1 + d12\ C1 \quad \ldots\ldots\ldots\ldots\ldots\ldots(17)$$

$$\Delta C = d21.C2 + d22.C2 \quad \ldots\ldots\ldots\ldots\ldots\ldots(18)$$

where the d terms are the coefficients of the inverse of the matrix

$$\begin{bmatrix} b11 & b12 \\ b21 & b22 \end{bmatrix}$$

e) Using the calculated values of the parameters, the process involving steps a) to d) was repeated, giving a new inverse matrix and readjusted parameters. The iteration was repeated until the change in the parameters was less than .01% of the parameter values.

From the final inverse matrix, the errors of the parameters were calculated:

$$\sigma^2(A_{10}) = d11 \cdot \sigma_o^2 \quad \ldots\ldots\ldots\ldots\ldots\ldots\ldots\ldots(19)$$

$$\sigma^2(C) = d22 \cdot \sigma_o^2 \quad \ldots\ldots\ldots\ldots\ldots\ldots\ldots\ldots(20)$$

σ_o^2 is called the 'unit variance' and was calculated from

$$\sigma_o^2 = S/\text{(Number of degrees of freedom)} \quad \ldots\ldots(21)$$

S is the sum of the squares of the weighted residuals at each point and the number of degrees of freedom are the total number of data points minus the number of parameters being determined.

The steps outlined above were written in Elliot Algol and the program was run on the Elliot 803 computer at the University of Kent at Canterbury. Data required were the total number of data points, the initial parameter estimates together with the half-lives of the known components in the decay. The time, activity and total number of counts observed were then read in for each point.

The output was arranged so as to give the parameter values together with their calculated errors. Warnings

were also incorporated to show which points lay more than 5% of their activity value from the smooth curve. The calculated and observed activity readings for each point were also printed out for detailed comparison.

The decay system which found the greatest application was the simplest:

$$At = A_{1o}\, e^{-\lambda_{1}t} + C.$$

This equation was applied whenever there was a single main decay apparent and the other components had half-lives such that they could be considered constant during the decay of the short activity. It was found unnecessary to put strict limits upon these requirements: the effect of forcing a complex decay to follow a too simple equation was that unrealistic values for one or more of the parameters resulted. For example, negative activities or negative half-lives might be found.

As it was desired to analyse the data on a routine basis, logical steps were incorporated into the program to eliminate bad data points. 'Bad' in this sense meant wildly

inaccurate points due to (for example) counting-equipment malfunction or computer reading errors. The criteria employed to judge data points were quite arbitrary. The activity of the observed point was required to differ from the calculated value by at least 10% of its value or by 10 standard deviations before a point was rejected. It was also found advisable to carry out a primary selection giving all points unit weighting to eliminate the otherwise common occurrence of an incorrect point with an incidentally large weighting causing better points with lower weights to be rejected instead.

This data-rejection process was found useful only for the single component case: frequently an imbalance set in when it was applied to the double component cases causing the rejection of too many data points. In these cases, graphical inspection of the decay data before and after analysis was employed.

The standard deviations for typical analyses of single-component data were 1 to 2%. Those for the two-component analyses were a little larger: 2 to 4%. The explanation

for this is probably that in the first place, more information was being extracted from the two-component data and in the second, counting was continued over a longer time span thus allowing long-term equipment drift to have a greater effect on the data.

A simplified flow-diagram of the programs is shown in figure (4.1). The box labelled 'CYCLE' is shown in greater detail in figure (4.2) as this contains the main working of the least-squares solution. The program used for the single component decay analysis is given in full in Appendix B.

Computer Program for the Analysis of Single Component Decays by the Method of Lease-Squares

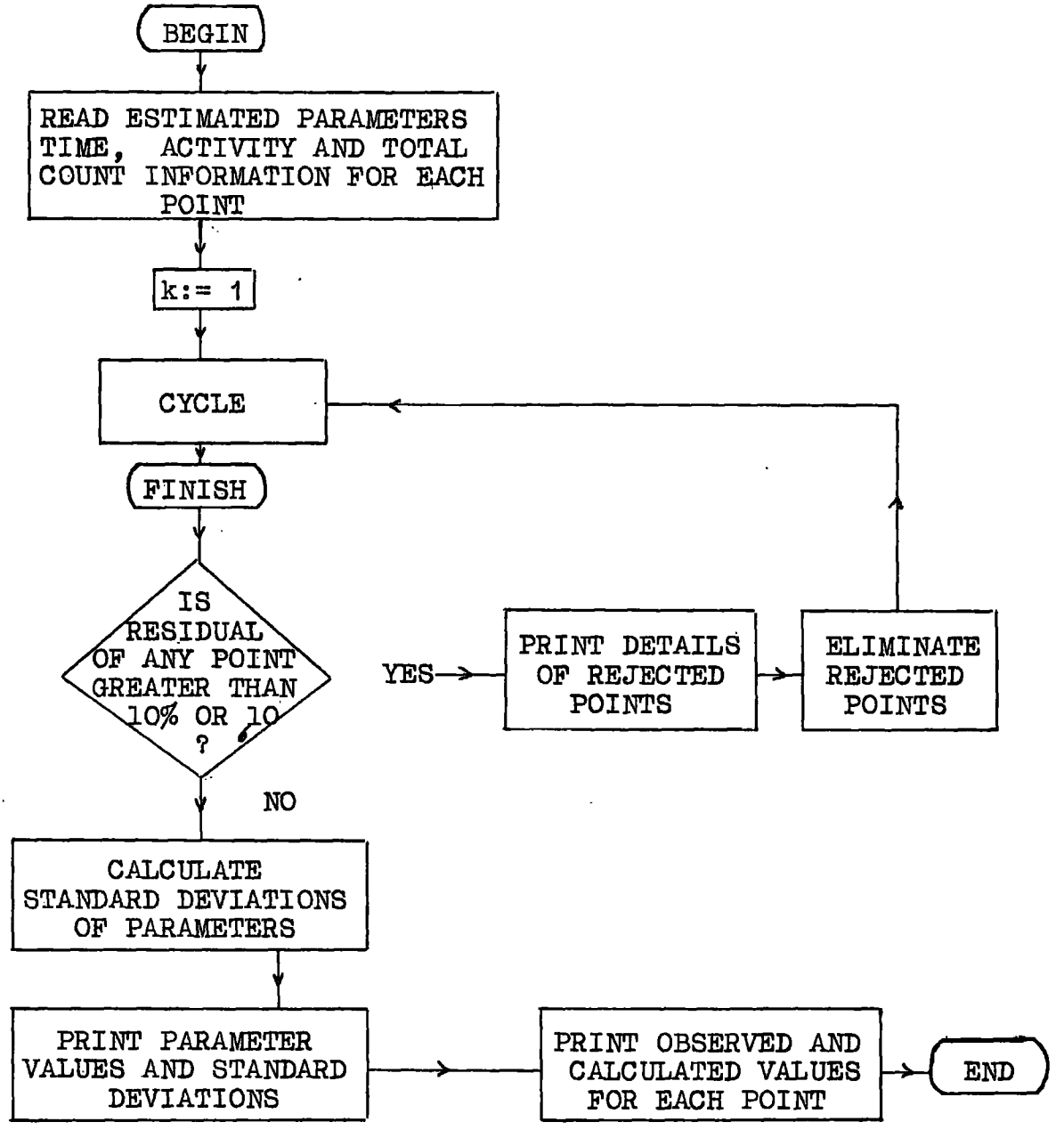

Figure 4.1

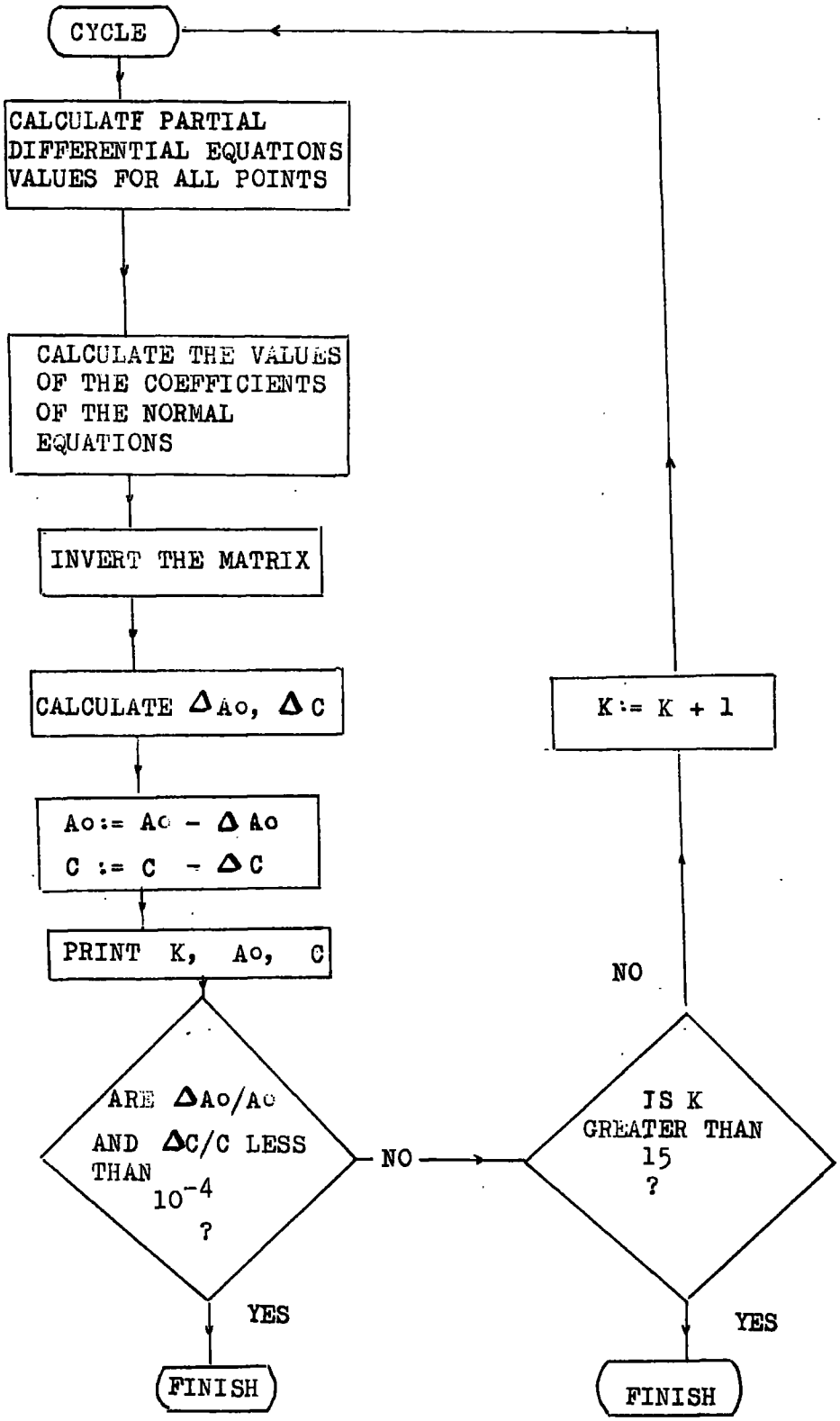
CYCLE
CALCULATF PARTIAL DIFFERENTIAL EQUATIONS VALUES FOR ALL POINTS
CALCULATE THE VALUES OF THE COEFFICIENTS OF THE NORMAL EQUATIONS
INVERT THE MATRIX
CALCULATE ΔAo, ΔC
Ao:= Ao - ΔAo
C := C - ΔC
PRINT K, Ao, C
ARE ΔAo/Ao AND ΔC/C LESS THAN 10^-4 ?
NO
YES
FINISH
IS K GREATER THAN 15 ?
NO
YES
FINISH
K:= K + 1

Figure 4.2

Chapter 5

Results and Discussion

a) Introduction.

The treatment of the experimental results to give first relative and then absolute yields which are compared with previously published values is set out in this chapter. Prompt neutron yields are estimated from complementary mass yields and changes occuring on the 'wings' of the asymmetric yield peaks with change in the initial excitation energy are noted. The results are discussed.

b) Calculation of Relative Yields

Consider an irradiation in which the isotope 'A' isolated is part of the β -decay chain:

$$\text{short} \longrightarrow A \xrightarrow{\lambda_A} \text{stable}$$

if the rate of production of A at any time t during the irradiation is $R_t = \frac{dN_A}{dt}$.

then at time t after the end of the irradiation

$$dN_A = R_t.dt.\ \exp(-\lambda_A(t' + T - t))$$

where T is the length of the irradiation. Integrating this expression over the whole irradiation gives

$$N_A(t') = \int_0^T R_t.\ \exp(-\lambda_A(t' + T - t))\ dt$$

$$= \exp(-\lambda_A.t') \int_0^T R_t.\ \exp(-\lambda_A(T - t))\ dt.$$

The rate of production of A, R_t, is proportional to the fission cross-section, σ, the fission-yield of A, Y_A, and the instantaneous flux reading, I_t.

Thus $R_t = C.\sigma.\ Y_A.\ I_t$

The constant of proportionality, C, includes the efficiency of the counter monitoring the neutron flux.

Substituting for R_t:

$$N_A(t') = C.\sigma.\ Y_A.\ \exp(-\lambda_A.t') \int_o^T I_t.\ \exp(-\lambda_A(T-t))dt.$$

The observed neutron flux, I_t, is irregular in nature and the integral cannot be evaluated directly but may be approximated by the summation

$$S_A = \sum_{t=o}^{T} I_t.\ \exp(-\lambda_A(T-t)).\ \delta t$$

provided that the periods δt are much shorter than the half-life of A and the duration of the irradiation.

Replacing the integral by S_A gives

$$N_A(t') = C.\sigma.\ Y_A.\ \exp(-\lambda_A.t').\ S_A$$

and the yield of A at $t' = o$ is

$$Y_A = \frac{NA}{C.\sigma.\ S_A} = \frac{A_A^{\ o}}{C.\sigma.\ \eta_A.\ \lambda_A.\ S_A},$$

where A^o_A is the observed activity at $t' = o$ and η_A the counter efficiency.

The relative yield of A may therefore be expressed as

$$\frac{Y_A}{Y_R} = \frac{A_A^{\ o}.\ \eta_R.\ \lambda_R.\ S_R}{A_R^{\ o}.\ \eta_A.\ \lambda_A.\ S_A} \qquad \ldots\ldots\ldots\ldots\ 5.1$$

The subscript 'R' refers to the reference isotope in this equation.

The more usual case is where the isotope B in the following mass-chain is isolated and measured:

$$\text{short} \longrightarrow A \xrightarrow{\lambda_1} B \xrightarrow{\lambda_2} \text{stable}.$$

It is assumed that B has a longer half-life than A and that all B is formed by decay of A.

A similar argument to that in the previous example gives

$$N_B(t') = \frac{\lambda_A}{\lambda_B - \lambda_A}\left[e^{-\lambda_A t'}\int_0^T R_t \cdot \exp(-\lambda_A(T-t))dt - \exp(-\lambda_B t')\int_0^T R_t \cdot \exp(-\lambda_B(T-t))dt\right]$$

$$\text{ie } N_B(t') = C \cdot \sigma \cdot Y_A \cdot \frac{\lambda_A}{\lambda_B - \lambda_A}(\exp(-\lambda_A \cdot t') \cdot S_1 - \exp(-\lambda_B \cdot t') \cdot S_2)$$

If the decay observations are made when all A has decayed away so that $\exp(-\lambda_A t') \longrightarrow 0$, then

$$N_B(t') = C \cdot \sigma \cdot Y_A \cdot \frac{\lambda_A}{\lambda_A - \lambda_B} \cdot S_2 \cdot \exp(-\lambda_B \cdot t') \text{ and}$$

$$N_B^{\circ} = C \cdot \sigma \cdot Y_A \cdot \frac{\lambda_A}{\lambda_A - \lambda_B} \cdot S_2 \quad .$$

The equivalent to equation 5.1 is then

$$\frac{Y_B}{Y_R} = \frac{A_B^{\circ}}{A_R^{\circ}} \cdot \frac{\lambda_R}{\lambda_B} \cdot \frac{\eta_R}{\eta_B} \cdot \frac{S_R}{S_B} \cdot \frac{\lambda_A - \lambda_B}{\lambda_A} \quad \ldots\ldots\ldots 5.2$$

c) Calculation of Absolute Yields

While the isotopes measured had been chosen so as to lie towards the stable ends of the β -decay chains, in certain cases, corrections for the independent yields of the isobars occuring later in the chains than those separated had to be applied.

The problems entailed in making these corrections have been discussed in chapter 1. An outline of the correction process follows.

The complementary mass of the measured isotope was calculated from

$$A^* = A_f - \nu - A \quad \text{.....5.3}$$

Values for the most stable charges associated with these fragments have been tabulated by Coryell[5.1].

The most probable charge was calculated from the equation

$$Zp = Z_A - \tfrac{1}{2}(Z_A + Z_A^* - Zf)$$

which was given in chapter 1 and this was then applied to the empirical probability curve given by Wahl[5.2].

The values of $\bar{\nu}$, the prompt neutron yield, for each energy were taken from a table prepared by Leachman[5.3]; they were 2.75 for 3 MeV and 4.75 for 14.8 MeV neutron irradiations.

The results of the calculations of the independent yields of later members of the decay chains are not set out in detail here because for all of the isotopes separated except Sb^{129}, more than 99.99% of the yield for each chain was included at the isotope at which the measurement was based. For Sb^{129} the percentage of the total chain yield separated was calculated to be 99.93% and 99.52% for irradiations employing 3 MeV and 14.8 MeV neutrons respectively.

The corrected relative yield values were transformed to absolute yields by taking published values for the absolute yield of Mo^{99}. Walker[5.4] has reviewed yield values for U^{238} fission with fission-spectrum and 14 MeV neutrons and has selected best values for the absolute yield at mass 99. His values (6.32% and 5.68% for fission-spectrum and 14 MeV neutrons respectively) were then used to relate relative fission yield data from several sources.

Since the publication of this review, yields for several mass-chains based on absolute measurements of the yield at mass 99 have been published by Bonyushkin et. al[5.5] and Petrzhak et. al[5.6]. The value of the yield of at mass 99 from irradiations with fission-spectrum neutrons given by Bonyushkin, 7.0 $\pm$ .7% is appreciably higher than the value adopted by Walker but in view of

the large error associated with their measurement there seems to be no good reason for the adoption of a value higher than 6.32%.

For irradiations with 14 MeV neutrons, the yields for mass 99 given by Bonyushkin et al[5.5] and Petrzhak et al[5.6] namely 6.5 ± .5% and 6.4 ± .7% are again higher than the value of 5.68% adopted by Walker. However, the mass-yield curve constructed by Walker using this yield value and applying it to relative yield values of Bloom[5.8], Protopopov et al[5.7], Cuninghame[5.10] and Ford et al[5.11] was satisfactory judging by the total percentage yield under the curve.

The values taken by Walker for the yields at mass 99 have therefore been used in this work in the conversion from relative to absolute yields.

d) Results and Discussion

The results of the relative yield measurements are set out in tables 5.1 to 5.8. The errors quoted are the standard deviations of the observations. The absolute yields, obtained as discussed above, are given in table 5.9.

The mass-yields from the irradiations using 3 MeV neutrons have been plotted in figure 5.1. A smooth curve, drawn through the yields collected by Walker[5.4] and the

Table 5.1 Relative yields for Sr^{91}

isotope /Run	A^o	chemical efficiency	η(Sr)	η(Ym)	η^{1*}	S	Rel. Yield	E(n)
Sr 1	733	18.15%	33.7%	34.0%	34.69	8.3005	.563	3
Mo 1	420	39.90	34.10			8.5675		
Sr 2	3446	58.94	32.6	33.8	33.58	1.1938	.558	3
Mo 2	1251	81.80	32.8			1.2320		
Sr 3	1122	25.34	33.5	34.0	34.49	8.2296	.539	3
Mo 3	622	51.90	33.7			8.4946		
Sr 4	3920	40.50	33.0	33.9	33.99	1.0001	.585	14
Mo 4	1553	65.94	33.3			1.0005		
Sr 5	14317	18.17	33.7	34.0	34.69	3.7049	.632	14
Mo 5	13386	77.84	32.9			3.7240		
Sr 6	34896	68.21	33.5	34.0	34.49	7.1813	.685	14
Mo 6	4493	41.64	34.1			7.2539		

* $\eta^1 = \eta(\mathrm{Sr}) + 0.0297\ \eta(\mathrm{Y^m})$

Average Sr^{91} relative yield (3 MeV) = 0.5533 ± 0.0126

(14 MeV) = 0.6340 ± 0.0501

Table 5.2 Relative Yields for Y^{93}

Isotope /Run	A^o	chemical yield	counter efficiency	S	Rel. Yield	E(n)
Y 1	4250	31.40	38.10	1.9595	.743	3
Mo 1	1786	69.61	35.00	2.0186		
Y 2	2447	42.28	38.00	1.3803	.768	3
Mo 2	687	63.51	35.40	1.4296		
Y 3	2064	34.61	38.10	5.6767	.752	3
Mo 3	782	69.98	35.00	5.8569		
Y 4	12667	21.02	38.20	3.6788	.770	14
Mo 4	6925	63.90	35.30	3.7039		
Y 5	8800	11.34	38.30	2.7980	.7835	14
Mo 5	7408	54.13	35.40	2.8120		
Y 6	1739	14.54	34.10	1.7984	.741	14
Mo 6	1553	65.94	33.30	1.8074		

Mean relative yield of Y^{93} (3 MeV) = $0.754 \pm .0128$

(14 MeV) = $0.765 \pm .0215$

Table 5.3 Relative Yields for Ru^{105}

Isotope /Run	A^o	chemical efficiency	γ^*	S	Rel. Yield	E(n)
Ru 1	4110	51.60	37.5	7.4307	0.534	3
Mo 1	279	29.24	34.5	7.9936		
Ru 2	4858	70.00	37.3	8.7680	0.596	3
Mo 2	97	12.80	35.0	9.4221		
Ru 3	5283	57.00	37.8	8.9592	0.675	3
Mo 3	105	11.88	35.0	9.6420		
Ru 4	2563	30.00	38.7	8.4523	0.528	3
Mo 4	776	82.06	32.8	9.0316		
Ru 5	3296	24.37	39.10	8.6020	0.677	3
Mo 5	7655	65.57	33.30	9.1347		
Ru 6	3350	15.70	39.64	9.3807	0.610	14
Mo 6	1062	54.63	33.70	9.4886		
Ru 7	6794	37.25	36.32	5.1776	0.737	14
Mo 7	697	46.36	33.90	5.2140		
Ru 8	17433	27.38	37.77	2.4923	0.607	14
Mo 8	1793	28.79	34.50	2.5063		

γ^* corrected for $Rh^{105\ m}$.

Average Ru^{105} relative yield (3 MeV) = $0.602 \pm .072$
(14 MeV) = $0.651 \pm .074$

Table 5.4 Relative Yields for Rh^{107}

Isotope /Run	A^o	Chemical Yield	?	S	Rel. Yield	E(n)
Rh 1	6659	27.95	33.8	4.3583	0.267	3
Mo 1	131	20.98	34.8	6.7685		
Rh 2	12671	32.56	33.7	1.3000	0.205	3
Mo 2	568	43.50	34.0	2.0246		
Rh 3	10786	29.40	33.9	1.1550	0.215	3
Mo 3	694	59.38	33.5	1.8285		
Rh 4	3676	13.35	34.0	1.1552	0.174	3
Mo 4	577	55.63	33.7	1.7414		
Rh 5	196252	40.10	33.7	2.0098	0.344	14
Mo 5	1897	27.70	34.6	2.1520		
Rh 6	100610	15.62	34.0	2.8638	0.380	14
Mo 6	2379	29.00	34.5	3.1215		
Rh 7	131570	38.86	33.70	2.1121	0.377	14
Mo 7	1557	36.03	34.20	2.2867		

Average Rh^{107} relative yield (3 MeV) = 0.215 ± 0.039
(14 MeV) = 0.367 ± 0.020

Table 5.5 Relative Yields for Sb^{129}

Isotope /Run	A^o	Chemical Yield	observed ?	γ_{56}	S	Rel. Yield	E(n)
Sb 1	956	46.82	40.8	87.4	6.5891	0.0571	3
Mo 1	628	66.64	33.3		7.0832		
Sb 2	160.8	5.12	41.3	88.25	1.1431	0.0519	3
Mo 2	1251	80.34	32.8		1.2320		
Sb 3	1208	51.49	40.3	86.12	7.8777	0.0519	3
Mo 3	622	51.90	32.9		8.4946		
Sb 4	596	28.34	41.0	87.60	1.5496	0.0465	3
Mo 4	280	22.57	34.7		1.6676		
Sb 5	56886	46.15	40.6	86.76	3.8173	0.243	14
Mo 5	4825	36.55	34.30		3.9028		
Sb 6	12838	30.63	41.0	87.61	2.4300	0.195	14
Mo 6	1305	23.57	34.6		2.4604		
Sb 7	17241	45.71	40.9	88.4	1.9016	0.237	14
Mo 7	2134	49.77	33.8		2.0610		
Sb 8	35080	52.07	40.8	87.2	8.4815	0.229	14
Mo 8	5514	75.14	33.0		8.6896		

Average Sb^{129} relative yield (3 MeV) = 0.0519 ± 0.0043

(14 MeV) = 0.226 ± 0.0215

Table 5.6 Relative Yields for I^{131}

Isotope /Yield	A^o	η	Chemical Yield	S	Rel. Yield	E(n)
I 1	92.0	31.70	41.67	1.5107	.495	3
Mo 1	853.0	33.50	62.90	1.5028		
I 2	67.7	31.30	67.17	1.3219	.465	3
Mo 2	539.0	32.8	82.43	1.3152		
I 3	50.8	30.30	53.13	1.0037	.501	3
Mo 3	189.0	34.50	30.13	1.0004		
I 4	51.4	30.70	37.97	1.0974	.503	3
Mo 4	582.0	33.20	69.41	1.0917		
I 5	1976	31.10	69.44	8.1255	.980	14
Mo 5	6046	33.3	67.30	8.1116		
I 6	2584	31.3	59.34	1.1770	.825	14
Mo 6	8827	33.7	53.79	1.1749		
I 7	2130	31.60	36.60	6.1232	.806	14
Mo 7	18250	32.80	84.24	6.1178		
I 8	2120	31.80	45.70	5.8504	.772	14
Mo 8	13731	76.15	76.15	5.8450		

Average I^{131} relative yield (3 MeV) = $0.491 \pm .0175$

(14 MeV) $0.846 \pm .092$

Table 5.7 Relative Yields for Ce^{143}

Isotope /Run	A^o	γ	Chemical Yield	S	Rel. Yield	E(n)
Ce 1	1974	30.8	52.88	2.0079	.839	3
Mo 1	1733	33.4	69.61	2.0816		
Ce 2	599	30.7	37.66	1.3893	.834	3
Mo 2	677	33.5	63.51	1.4296		
Ce 3	321	33.00	11.10	2.8739	.725	3
Mo 3	1316	33.3	65.32	2.8903		
Ce 4	262	31.60	13.35	1.6589	.854	3
Mo 4	285	34.7	22.57	1.6676		
Ce 5	4786	28.40	45.05	3.0772	.758	14
Mo 5	4814	33.6	58.31	3.0798		
Ce 6	24935	28.5	62.50	1.7450	.881	14
Mo 6	17410	33.3	66.01	1.7480		
Ce 7	465	32.7	17.78	1.3428	.861	14
Mo 7	1166	32.9	76.27	1.3497		
Ce 8	5558	31.7	45.50	3.4420	.766	14
Mo 8	5506	33.3	65.56	3.4686		

Average Ce^{143} relative yield (3 MeV) = $0.813 \pm .059$

(14 MeV) = $0.817 \pm .063$

Table 5.8 Relative Yields for Pr^{145}

Isotope /Run	A^o	γ	Chemical Yield	S	Rel. Yield	E(n)
Pr 1	3825	34.0	54.5	1.3410	0.6125	3
Mo 1	677	33.5	63.51	1.4296		
Pr 2	2129	34.0	28.30	8.1131	0.674	3
Mo 2	420	34.1	40.12	8.5670		
Pr 3	5294	34.0	30.15	1.9122	0.648	3
Mo 3	1733	33.4	69.61	2.0186		
Pr 4	23138	34.0	44.02	2.0189	0.517	14
Mo 4	5289	33.6	58.99	2.0367		
Pr 5	20712	34.0	38.49	3.0530	0.575	14
Mo 5	4814	33.6	58.31	3.0798		
Pr 6	34130	34.0	53.64	3.6582	0.547	14
Mo 6	6566	33.5	63.9	3.7039		

Average Pr^{145} relative yield (3 MeV) = $0.645 \pm .030$

(14 Mev) = $0.547 \pm .029$

Table 5.9

Absolute Yields of Isotopes from U^{238} bombarded with 3 MeV and 14.8 MeV Neutrons

Mass Chain	3 MeV*	14.8 MeV**
91	3.50 ± 0.08	3.60 ± 0.28
93	4.77 ± 0.08	4.33 ± 0.12
105	3.81 ± 0.46	3.70 ± 0.42
107	1.36 ± 0.25	2.08 ± 0.11
129	0.329 ± 0.027	1.29 ± 0.12
131	3.10 ± 0.11	4.81 ± 0.52
143	5.14 ± 0.37	4.64 ± 0.36
145	4.08 ± 0.19	3.11 ± 0.16

* Taking the absolute yield at mass 99 to be 6.32%.

** Taking the absolute yield at mass 99 to be 5.68%.

yields by Bonyushkin et al[5.5] and Petrzhak et al[5.6](all points were renormalised relative to a mass 99 value of 6.32%) have been included.

The mass-yields from the irradiations using 14.8 MeV neutrons have been plotted in figure 5.2. The smooth curve was drawn through the data collected by Walker, taking into account also the mass-yields measured by Bonyushkin et al Petrzhak et al and James, Martin and Silvester[5.7]. The yields obtained by Bonyushkin et al. and Petrzhak et al. were renormalised relative to a mass 99 value of 5.68%. , but the results due to James, Martin & Silvester had been measured relative to mass 139 and as their absolute yield (4.92%) at this mass agrees closely with the value given by Walker for mass 139 (4.90%) their values were used directly and without further renormalisation.

The fit of the points to the curves appears satisfactory for the mass yields obtained using both 3 MeV and 14.8 MeV neutrons, although it should be pointed out that the spread of the published yields may be large for any given mass and that the detailed shapes of the mass-yield curves obtained using neutrons of both energies are as yet fairly uncertain.

The yields observed in this work at both neutron energies have been plotted in figure 5.3. 'Centroid'

Absolute Mass-Yield from the Fission of U^{238} irradiated with Fission Spectrum and 3 MeV neutrons.

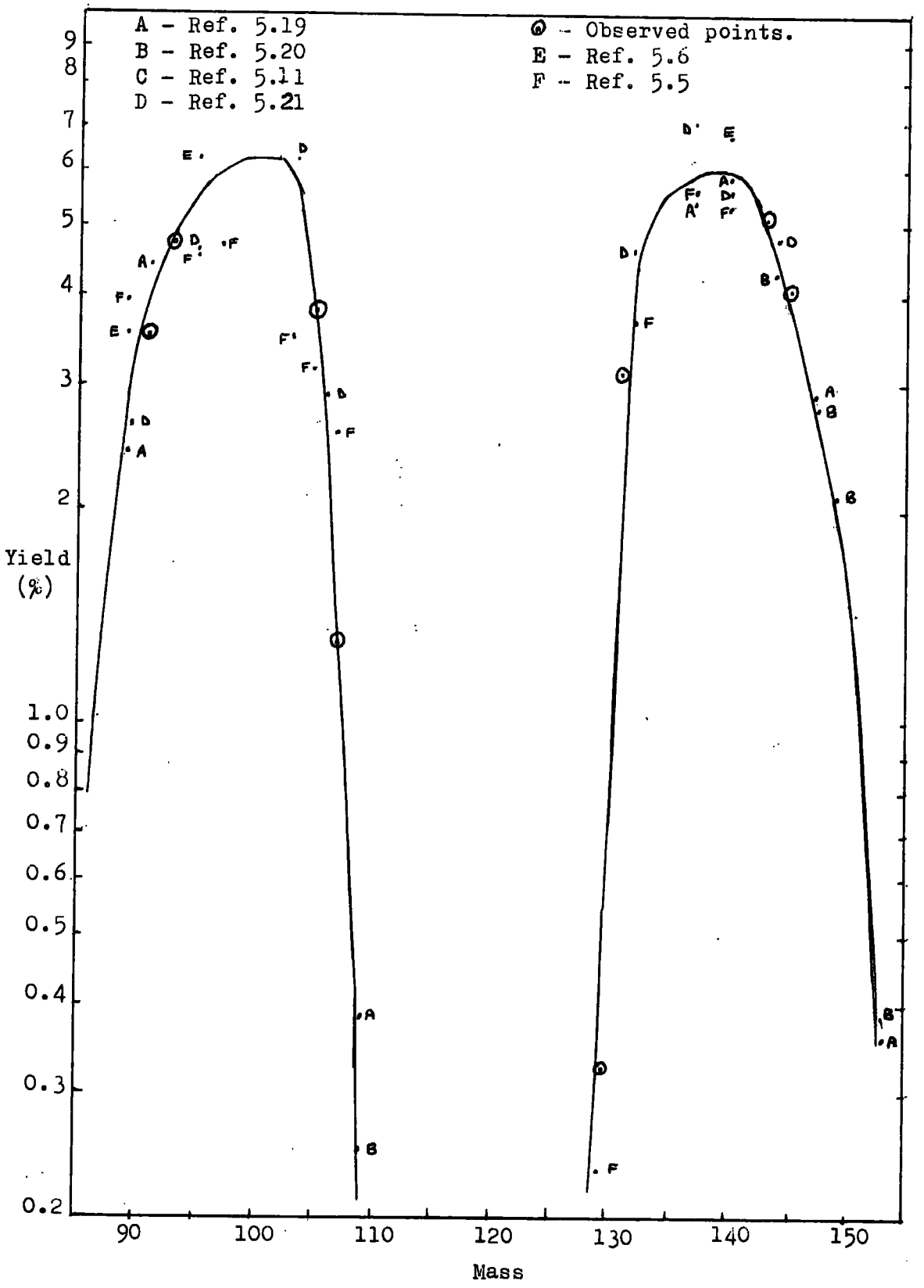

Figure 5.1

Absolute Mass-Yields for the Fission of U^{238} irradiated with 14.8 MeV neutrons.

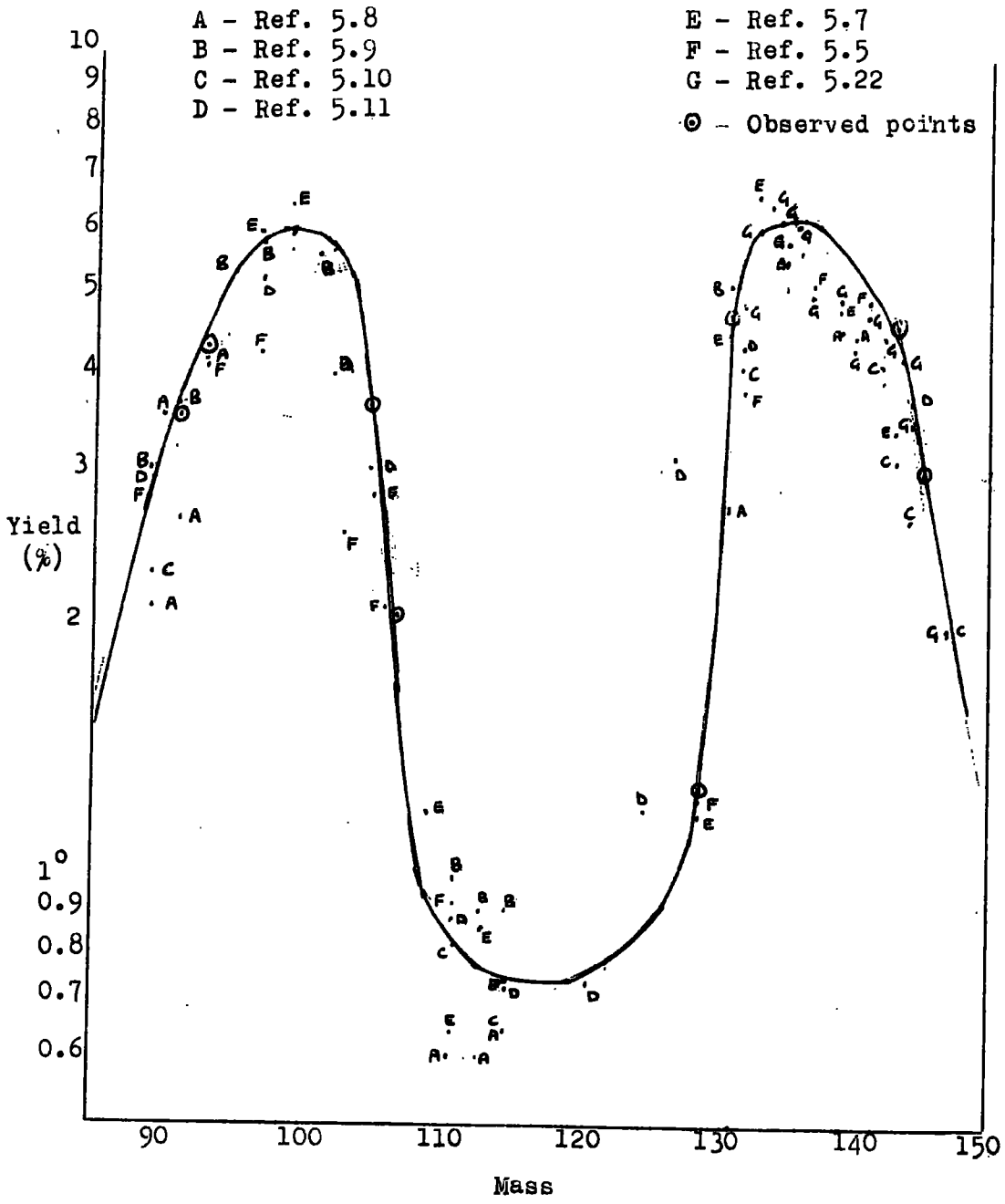

Figure 5.2

peak positions calculated using the yields measured in this work are at masses 98.2 and 138.6 for the irradiations with 3 MeV neutrons and at 98.3 and 137.1 for the irradiations using 14.8 MeV neutrons.

It is apparent from these values and from figure 5.3 that the light and the heavy peak have responded differently to the change in the excitation energy. The light peak shows little change in position between the two energies although the increase in the symmetrical and highly asymmetrical mass yields at the greater excitation energy is reflected by the decrease in the slopes of this peak for the 14.8 MeV compared to the 3 MeV irradiations.

The heavy peak shows different behaviour. The slopes of the wings of this peak change little between the two excitation energies but the peak appears to have moved to a lower mass value at the higher excitation energy. This trend has previously been noted and commented upon by Rahman[5.12] for thorium-232 bombarded by 3 and 14.8 MeV neutrons.

Such a movement is contrary to observations made on various fissioning nuclei at the same excitation energy[5.17] which shows that the inner wing of the heavy peak remains fixed in position and that the light peak moves to higher or lower mass positions depending on the

Comparison of Observed Mass-Yields of U^{238} excited by 3MeV and 14 MeV neutrons.

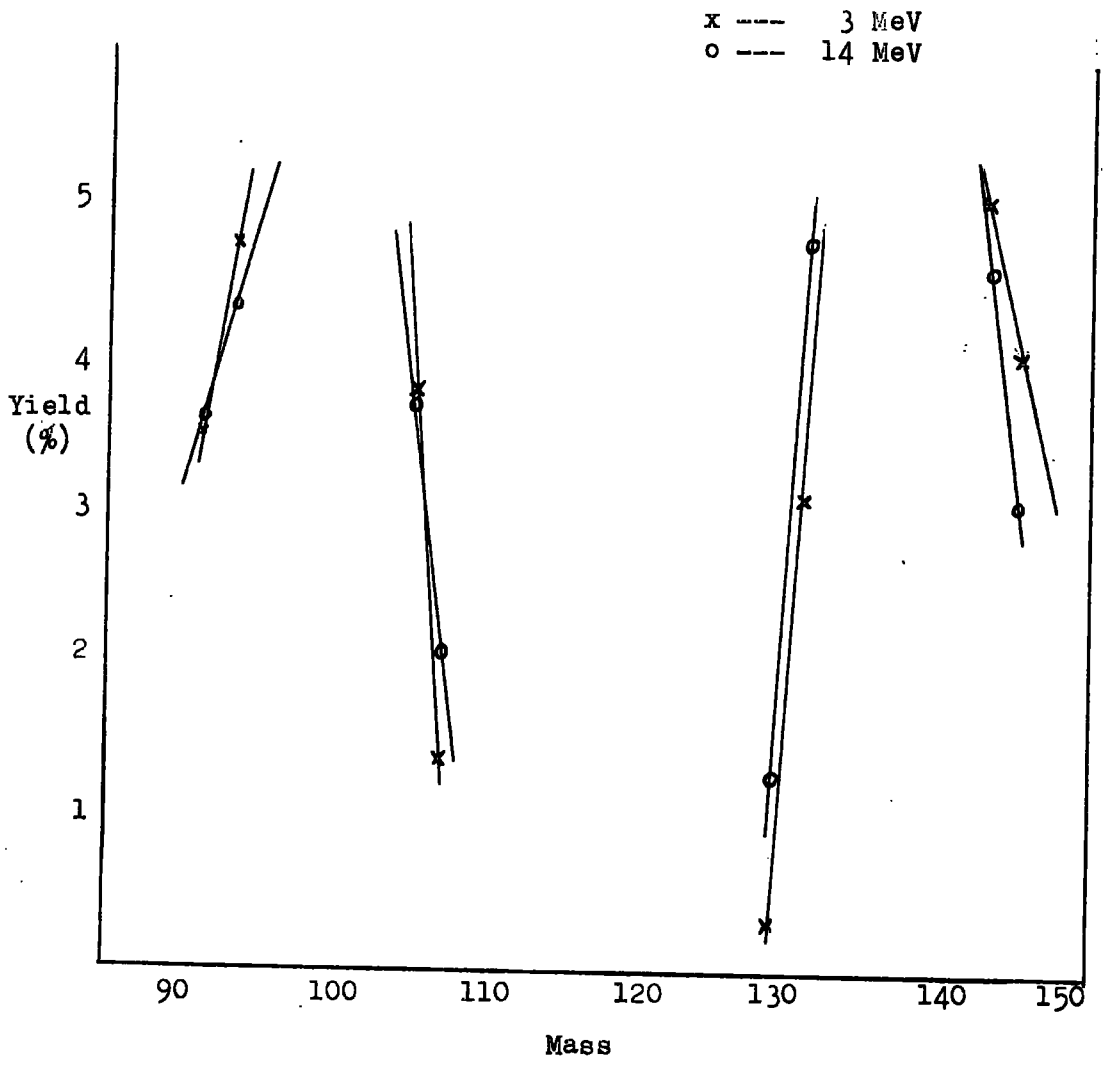

Figure 5.3

mass of the fissioning nucleus.

Comparison of the slopes of the edges of the peaks has been made in table 5.10. Values of Δ(yield)/Δ(mass) are tabulated for each pair of measured yield values on the sides of the peaks. Table 5.10 shows clearly that at both bombarding energies, the inner edge of the heavy peak has the greatest slope.

The numbers of prompt neutrons associated with pairs of fission products are given in table 5.11. In each case a mass chain whose complementary fragment lies between two measured mass yields has been taken. The mass of the complementary fragment was calculated from the masses and yields of the chosen mass chain and the masses and yields on either side of the complementary fragment.

The prompt neutron yields from the 3 MeV neutron irradiations are fairly consistent with each other. Those from the irradiations employing 14.8 MeV neutrons are of interest however because of the variation of prompt neutron yields, depending on the pairs of fission products taken.

The errors in these values are given in parentheses in table 5.11. They were calculated from the standard errors of the observed mass yields, where the standard error was taken to be the standard deviation of the yields (as given in table 5.9) divided by the square root of the number of repeated observations contributing to each mean yield

Table 5.10

The Slopes of the Edges of the Light and the Heavy Mass-Yield Peaks

Energy of bombarding neutrons		Inner Slope*	Outer Slope*
Light Peak	3 MeV	1.225(0.241)	0.635(0.066)
	14.8 MeV	0.810(0.251)	0.365(0.176)
Heavy Peak	3 MeV	1.39 (0.06)	0.530(0.216)
	14.8 MeV	1.76 (0.27)	0.765(0.204)

* Errors in parenthesis were calculated from the standard errors of the mass yields.

Table 5.11

The number of secondary neutrons, ν, associated with fission-product pairs

Energy of bombarding neutrons	Fission-product mass	Mass of complementary fission-product	ν*
3 MeV	93	143.83	2.17(0.24)
	107	129.71	2.29(0.09)
	131	105.57	2.43(0.13)
	145	91.97	2.03(0.19)
14.8 MeV	91	144.36	3.64(0.24)
	93	143.41	2.59(0.21)
	105	130.37	3.63(0.17)
	107	129.45	2.55(0.06)

* Errors in parentheses were calculated from the standard errors of the mass yields.

value. It is apparent that the variation in ν for the irradiations using 14.8 MeV neutrons is much greater than can be accounted for by these errors.

The shift in the position of the heavy mass-yield peak can be plausibly explained on a qualitative basis from a consideration of the number of prompt neutrons emitted by the fission fragments as a function of the excitation energy of the compound nucleus.

Measurements of the number of prompt neutrons emitted during fission as a function of fragment mass ($\nu(M)$) have been made for thermal neutron induced fission of U^{235} and U^{233} by Apalin et al[5.13] and Milton and Fraser[5.14]. Measurements of $\nu(M)$ for the spontaneous fission of Cf^{252} and a series of calculations by Terrell using pre-neutron-emission and post-neutron-emission data have shown that the resulting function of $\nu(M)$ is remarkably similar for several different fissioning systems[5.15,5.16].

These curves of $\nu(M)$ show a steady increase in ν as the fission-fragment mass increases across the light mass-yield peak reaching a maximum value at about mass 115; ν then decreases to a pronounced minimum at about mass 130 before finally rising again across the heavy peak.

Few measurements of $\nu(M)$ have been made for fissioning systems which have acquired greater excitation energies than those obtained using thermal neutrons. However,

recently, two studies of $\nu(M)$ for the fission of heavy nuclei having excitation energies comparable to those obtained in the present work have been published.

Cheifetz and Fraenkel measured ν as a function of fission fragment mass for U^{238} bombarded by 12 MeV protons[5.18]. They compared their results with previously published measurements of $\nu(M)$ for the thermal neutron induced fission of Pu^{239}.

Their work shows that the dip in the $\nu(M)$ curve at about mass 130 becomes less pronounced for fission at the higher excitation energy and that proportionately more prompt neutrons are emitted by the heavy fragments than by the light fragments as the compound nucleus excitation energy is increased.

Burnett et al. measured $\nu(M)$ at two bombarding energies[5.23]. Comparison was made of the prompt neutron emission from fission of U^{233} bombarded by 8.5 and 13.0 MeV protons. They came to conclusions similar to those arrived at by Cheifetz and Fraenkel concerning the number of neutrons emitted by fragments of varying mass with a change in the bombarding energy. For fragments of the light mass peak, little or no change in $\nu(M)$ was observed with change in bombarding energy. A change, $\Delta\nu$, in $\nu(M)$ was observed however, for masses in the heavy peak region and the maximum $\Delta\nu = \nu(13\ \text{MeV}) - \nu(8.5\ \text{MeV})$ was found at around mass 130.

The results of Burnett et al. and Cheifetz and Fraenkel can be used to explain the observations of this work regarding the changes in the positions of the light and heavy mass-yield peaks with a change in the neutron bombarding energy. If at high bombarding energies, more prompt neutrons are emitted by the heavy than by the light fragments, then one effect of this would be a movement of the position of the heavy fission-product mass-yield peak to lighter mass values. Similarly, if the greatest increase in ν occurs at about mass 130 then the greatest shift in mass values would be expected for fission products lying on the inner edge of the heavy peak.

Vandenbosch has described the fission process using a shell model which explains qualitatively the shape of the $\nu(M)$ curve[5.24]. In this explanation the presence of the nuclear shells, 50 protons and 82 neutrons at mass 132 causes fragments close to this mass value to be spherical and relatively undistorted. One result of this is that the energy of fragments of this mass appears mainly as kinetic energy, whereas for fragments far from closed shell configurations the total fragment energy appears to a relatively greater extent as excitation energy. The dip in the sawtooth response of $\nu(M)$ at low compound-nucleus excitation energies is therefore, from the viewpoint of this model due to the doubly magic shell (Z=50, N=82) present in fragments of mass greater than 132.

It is noteworthy from table 5.10 that the slope of the inner edge of the heavy mass-yield peak is greater for fission induced with 14.8 than for those induced with 3 MeV neutrons. This is contrary to the change in the slope of the inner edge of the light peak. It is possible, in the light of the proceeding considerations, that the number of neutrons emitted by fragments of just above mass 132 is sufficiently great to counteract the effect of the 'peak to valley' ratio decreasing at the higher bombarding energy and cause the slope of the inner edge of the heavy-mass-yield peak to increase locally about mass 130.

For the irradiations employing 14.8 MeV neutrons, the numbers of prompt neutrons associated with fission products of masses 93 and 107 together with their complementary fission products at masses 143.3 and 129.5 are lower than the number associated with the remaining two pairs by approximately one neutron. They are in fact only slightly greater than the number of prompt neutrons associated with fission product pairs of similar masses emitted during the irradiations with 3 MeV neutrons.

These low ν values obtained from the irradiations with 14.8 MeV neutrons imply the possibility of systematic errors in one or more of the mass yields used in the calculation of ν. From the design of the experiments, it would appear unlikely that systematic errors of measurement

could effect mass yields obtained from irradiations using neutrons of one energy and not the other. Measurements at both energies were carried out close in time to minimise effects arising from the malfunctioning of equipment. Chemical separations were the same for the two sets of irradiations except for I^{131} for reasons given in Chapter 2. It should also be noted that the data leading to ν are independent of the value assigned to the absolute yield for mass chain 99.

Examining the pairs of fission products giving rise to the two low ν values in turn, it is apparent that the pair consisting of mass-chain 93 and its complement has an associated relatively large error. Comparison with the immediately preceding pair of mass yields in table 5.11 shows that the ν values for these two pairs are separated by only about 0.6 neutrons from the limits of their associated errors.

The yields of the three masses, 93, 143 and 145 used in the calculation of ν for the fission product at mass 93 and its complementary fragment are given in table 5.9. The yield at mass 143 has the greatest proportional standard deviation of these three and comparison of this yield with previously published values by Cuninghame (3.2%)[5.10], James, Martin and Sylvester (3.51%)[5.7] and Gorman and Tomlinson (4.26%)[5.22] indicated that the value obtained in the present work may be too high. A value of, say,

4.0% for the yield at this mass leads to a value of ν of 3.74. The value of ν for the fission product at mass 91 and its complementary fragment is effected by this alteration; ν becomes 4.10 instead of 3.64. The number of prompt neutrons for these pairs of fission products now agree within the error limits indicating perhaps that a systematic error does exist in the yield at mass 143 for the irradiations employing 14.8 MeV neutrons.

Values for the yield at mass 143 have not been published previously for irradiations of U^{238} with 3 MeV neutrons; a check on the mass-yield value obtained in this work for bombardments with such neutrons is therefore not possible. However, the value of ν for the fission product of mass 93 and its complementary fragment close to mass 143 (as shown in table 5.11) does not differ significantly from the other values for ν obtained from 3 MeV neutron induced fission.

It is possible to be more conclusive regarding the low ν value for 107 and its complementary mass obtained from the results of irradiations with 14.8 MeV neutrons. The low associated error is indicative of the small effect errors in yields at masses 107, 129 and 131 have on the value of ν. A doubling of the value of the yield at mass 129 is needed to give a value of ν of 3.5 and an increase in the yield of mass 131 by 30% to the highly unlikely value of 6.24% gives rise to a prompt neutron value of

only 2.68. Similarly, a 100% decrease in the yield at mass 107 results only in a ν value of 3.14.

Contrary therefore to the possible conclusion arrived at with respect to the fission products of mass 93 and its complementary fragment, it does not appear at all likely that the low value of ν obtained for mass 107 and its complementary fragment has its origin in errors of yield measurement, since quite exceptional changes in these mass yields are required to increase the value of ν to a significant extent.

Results published by Lyle, Martin and Rahman[5.26] which include values for the prompt neutron yields associated with pairs of fission products arising from the 3 and 14.8 MeV neutron bombardment of Th^{232} also show a low value of ν for a pair of fission products, one of which lies between masses 129 and 131, for bombardments with 14.8 MeV neutrons. This low value is not so pronounced as that obtained in the present work and it does not approach the values of ν obtained from their irradiations using 3 MeV neutrons. The difference may possibly be due to comparison of a neutron light (Th^{232}) with a more neutron rich (U^{238}) initial nucleus.

The value of 2.55 for ν for mass 107 and its complementary fragment obtained in the present work in irradiations employing 14.8 MeV neutrons is only slightly greater than the value obtained (2.29) when 3 MeV neutrons

were employed. It may be concluded that a relatively small increase in the number of prompt neutrons has occurred just below mass 131 when the neutron bombarding energy is increased from 3 to 14.8 MeV.

It was concluded in the discussion above on the comparison of the slopes and positions of the mass-yield peaks that a relative increase in the number of neutrons emitted by fission fragments of mass just greater than 132 was needed to explain the increase of the slope of the inner edge of the heavy mass yield peak. This statement is in accordance with the conclusion set out in the previous paragraph.

The observations made in this work regarding the inner edge of the heavy mass yield peak are satisfied by a pattern of prompt neutron emission which has the greatest increase in ν for fragment masses giving rise to fission products of mass 131 and above, combined with a small increase in ν for fragments giving rise to fission products of mass 130 and lower when the neutron bombarding energy is increased.

The curve of $\Delta\nu$ as a function of fission-fragment mass published by Burnett et al. for the curve of U^{233} bombarded by 8.5 and 13 MeV protons shows a maximum for $\Delta\nu$ at about mass $130^{5.23}$. However, the mass resolution in such measurements is poor relative to that obtained in the radiochemical work, thus preventing a detailed comparison

with the results from the present work. In addition, differences in the fissioning systems examined may mean that a strict comparison between them is somewhat suspect.

Appendix A

Details of Radiochemical Separations

All carrier solutions contained approximately 5 mg. $ml.^{-1}$ of the element concerned.

Strontium

Carrier solution

Strontium carbonate was dissolved in 2 M hydrochloric acid and standardised by the precipitation of strontium sulphate.[1]

Separation Procedure

(1) The irradiated uranyl nitrate was dissolved in 6 M nitric acid and 10 mg. quantities of the carriers of the elements to be isolated were added. 30 ml. of fuming nitric acid were then added and the solution was cooled to precipitate strontium nitrate.

(2) The precipitate from step (1) was dissolved in 1 ml. of water and strontium nitrate reprecipitated by the addition of 15 ml. of fuming nitric acid.

(3) The strontium nitrate was dissolved in 10 ml. of water and the solution was buffered by the addition of 1 ml. of

6 M acetic acid and 2 ml. of 6 M ammonium acetate. About 2 mg. of barium were added followed by 2 ml. of a 10% solution of potassium chromate and the solution was digested in a water bath for 10 minutes. The precipitate of barium chromate was centrifuged and discarded.

(4) A few drops of a saturated solution of sodium carbonate were added and the strontium carbonate precipitate centrifuged down.

(5) The strontium carbonate was dissolved in a few drops of dilute hydrochloric acid, a few drops of yttrium carrier were added and the pH of the solution was transferred to a separating funnel and shaken with 10 ml. of a 0.1 M solution of di(2-ethylhexyl)phosphoric acid (HDEHP) in petroleum ether. The aqueous phase was discarded and the organic phase washed twice with water. The strontium was back-extracted into 2 x 5 ml. of 0.1 M hydrochloric acid and finally precipitated as carbonate by the addition of sodium carbonate solution; strontium carbonate was mounted on a filter disc, washed with water and acetone and dried at 100°C.

Yttrium

Carrier Solution

Yttrium oxide was dissolved in a little concentrated hydrochloric acid and diluted with water. The solution was standardised by titration with EDTA using Xylenol Orange as indicator.[2]

Separation Procedure

(1) The uranyl nitrate was dissolved in 2 M hydrochloric acid and 10 mg. of each of the carriers for the isotopes to be separated were added. The fission-product solution was first oxidised with 2 drops of bromine and then reduced with 2 ml. of a 5% hydroxylamine hydrochloride solution.

(2) The rare-earth fluorides were precipitated in a polythene centrifuge tube by the addition of 2 ml. of concentrated hydrofluoric acid. The precipitate was dissolved using 2 ml. of water, 2 ml. of boric acid and 2 ml. of 6 M hydrochloric acid. (Step (2) was omitted if less than about 2 gm. of uranyl nitrate were present in solution.)

(3) Yttrium hydroxide, together with co-precipitated lanthanide hydroxides, was precipitated by the addition of 6 M ammonia solution; if uranium was present, sodium

carbonate was added to keep it in solution.

(4) The yttrium hydroxide was dissolved in 2 drops of 6 M hydrochloric acid. The solution was diluted to 10 ml. with water, transfered to a separating funnel and shaken with 10 ml. of 0.3 M HDEHP in petroleum ether. The organic phase was washed twice with 0.1M hydrochloric acid. The yttrium and rare-earths were then back-extracted by shaking the organic phase with 2 x 2ml. portions of concentrated hydrochloric acid.

(5) The aqueous phase from step (4) was passed through a 5 x 0.8 cm^2 ion-exchange column containing Deacidite FF, a strongly basic anion exchanger which had previously been equilibrated with concentrated hydrochloric acid. The column was washed with 2ml. of concentrated hydrochloric acid and all the washes were reserved.

(6) The effluent from step (5) was diluted with water and made alkaline by the addition of concentrated ammonia solution. Yttrium hydroxide was centrifuged down.

(7) The precipitate was dissolved in 10 ml. of 10 M nitric acid and 1ml. of 1 M potassium bromate solution. A few drops of cerium (III) carrier solution were added and the solution

was transfered to a separating funnel and shaken with 10 ml. of 0.3 M HDEHP in petroleum ether to extract cerium(IV). The aqueous phase was washed with petroleum ether and yttrium hydroxide precipitated by the addition of concentrated ammonia solution.

(8) The yttrium hydroxide was dissolved in a few drops of 6 M hydrochloric acid, diluted to 10 ml. with water and digested with 1 ml. of cation resin. The resin was placed on the column and yttrium and the rare-earths were eluted as described in chapter 3. Yttrium was precipitated as the oxalate by the addition of a few drops of a saturated solution of oxalic acid, collected on a filter disc, washed with water, alcohol and ether, and dried under vacuum.

Analysis of sources

The yttrium sources were determined by dissolving the sources in an acid solution containing ammonium persulphate and titrating with 0.01 M EDTA solution and Xylenol Orange indicator as described for cerium. (See page 122.)

Molybdenum

Carrier Solution

Molybdenum trioxide was dissolved in concentrated ammonia solution, diluted and acidified to yield a solution 2 molar in hydrochloric acid. The solution was standardised by precipitating the molybdenum (VI) with 8-hydroxyquinoline.[3]

Separation Procedure

(1) The uranyl nitrate was dissolved in 2 M hydrochloric acid and 10 mg. quantities of carriers for the isotopes to be separated were added. Redox reactions were carried out using bromine and hydroxylamine hydrochloride to promote isotopic exchange.

(2) Three ml. of a 5% solution of benzoin-α-oxime in ethanol were added and the mixture was poured into a separating funnel containing 50 ml. of ethyl acetate. After shaking the phases for one minute, the aqueous phase was poured off and kept for the separation of other elements.

(3) The organic phase was washed twice with 50 ml. of 1 M hydrochloric acid. The aqueous phases were each time discarded.

(4) 15 ml. of 5 M ammonia solution were added and the phases were shaken for 5 minutes to backextract molybdenum.

(5) The aqueous phase in a centrifuge tube was made just acid to Methyl Red with hydrochloric acid, a few drops of a 20 mg. $ml.^{-1}$ solution of Fe^{3+} were added followed by 1 ml. of concentrated ammonia solution. The ferric hydroxide precipitate was centrifuged down and discarded.

(6) The solution was made just acid to Methyl Red indicator using 6 M hydrochloric acid and the solution was then digested on a water-bath to remove traces of dissolved ethyl acetate. A 3% solution of 8-hydroxyquinoline in acetic acid was added slowly to slight excess and the precipitated $MoO_2(C_9H_6ON)_2$ was transferred to a filter disc, washed using warm water and ethanol and finally dried at 100°C.

Ruthenium

Carrier solution

Ruthenium chloride was dissolved in water and the solution made 1 M in hydrochloric acid.

Separation Procedure

(1) The uranyl nitrate or uranium oxide was dissolved in 2 M HCl and the carriers for the isotopes to be isolated

were added, Redox steps, digesting the solution in the presence of bromine and then hydroxylamine hydrochloride, were carried out to ensure isotopic exchange of ruthenium.

(2) Hydrogen sulphide was passed through the cooled solution and ruthenium was centrifuged down.

(3) The ruthenium sulphide was slurried with 6 M sulphuric acid and transferred to a distillation apparatus. 1 gm. of 'sodium bismuthate' was added and the flask was gently heated. Air bubbling through the flask transferred the distillate of ruthenium(VIII) oxide to the receiving flask which held 10 ml. of 12 M sodium hydroxide solution and which was cooled in an ice-bath.

(4) A few drops of iron(III) carrier solution were added and a ferric hydroxide scavenge was carried out.

(5) The solution separated from the precipitated iron was diluted to 30 ml., 5 ml. of ethanol were added and after digesting for a few minutes the ruthenium(IV) oxide precipitate was centrifuged down.

(6) The precipitate was slurried with water, transferred to a filter-disc, washed with water and ethanol and dried at 100°C.

Analysis of the samples remaining after counting

The ruthenium content of the samples remaining after counting were determined colorimetrically[4]: The sample was dissolved by warming in 10 ml. of concentrated hydrochloric acid. The volume of the solution was made up to exactly 100 ml. using concentrated hydrochloric acid and 5 and 10 ml. portions were pipetted into 25 ml. volumetric flasks. An equal volume of absolute ethanol was added followed by 5 ml. of an aqueous thiourea solution. The solutions were heated on a waterbath for 10 minutes and made up to the mark with a 1:1 $^{v}/_{v}$ solution of ethanol-hydrochloric acid. The absorbtion was measured at 620 mμ and compared with those given by a series of standards similarly prepared.

Rhodium

Carrier solution

Rhodium chloride was dissolved in water and made approximately 2 M in hydrochloric acid. The solution was standardised by precipitating the hexammino-cobalt(III) hexanitrato-rhodium(III) salt[3.14].

Separation procedure

(1) The uranyl nitrate was dissolved in 1 M hydrochloric acid, the appropriate carrier solutions were added and the solution digested in the presence of a few drops of bromine for 10 minutes. A saturated solution of sodium nitrite was added until no further reaction with acid was observed. The solution was digested a further 5 minutes.

(2) About 20 mg. of thallium(I) nitrate was added and the precipitate centrifuged down and washed with 10 ml. of 6 M hydrochloric acid.

(3) A few drops of concentrated hydrochloric and nitric acids were added to the precipitate which dissolved on warming. The solution was diluted to 10 ml. with water, boiled and excess saturated sodium nitrite solution was added. Thallium nitrate was stirred in as in step (2) and the precipitate collected by centrifugation.

(4) It was next dissolved in nitrate and hydrochloric acids and rhodium complexed with sodium nitrite as in step (3). The solution was made slightly acid to Methyl Red using hydrochloric acid and 3 ml. of a freshly prepared saturated solution of hexamino cobalt chloride was added. The

precipitate of hexammino-cobalt(III) hexanitrato-rhodium(III) was filtered through a filter-disc, washed with water and ethanol and dried at 120°C.

Antimony

Carrier solution

Antimony(III) chloride was dissolved in 2 M hydrochloride acid. The solution was standardised by precipitation as antimony(III) from homogeneous solution using ammonium thiocyanate as the source of sulphide ion.[3.15]

Separation Procedure

(1) The uranyl nitrate was dissolved in 2 M hydrochloric acid and 10 mg. quantities of the carriers of elements to be separated were added. The solution was digested for 10 minutes in the presence of bromine and then hydroxylamine hydrochloride.

(2) Two drops of ammonium sulphide were added to the cooled solution and antimony sulphide centrifuged down.

(3) The antimony sulphide precipitate was dissolved in 5 ml. of concentrated hydrochloric acid and the solution evaporated down to 2 ml. 8 ml. of water and 5 mg. of tellurium carrier solution were added followed by 1 ml. of

hydrazine hydrate solution and sulphur dioxide was passed into the warm solution. Tellurium metal was centrifuged down and discarded.

(4) Antimony sulphide was precipitated by the addition of a drop of ammonium sulphide solution and the precipitate collected by centrifugation: and dissolved in 10 ml. of concentrated hydrochloric acid.

(5) 1 ml. of di-isopropyl ether and 9 ml. of benzene were shaken with 10 ml. of concentrated hydrochloric acid and one drop of bromine. The aqueous phase was discarded and the antimony solution from step (4) was shaken with the di-isopropyl ether/benzene phase for 1 minute.

(6) The aqueous phase was discarded and the organic phase was washed by shaking twice with 2 ml. of concentrated hydrochloric acid. The aqueous washings were discarded.

(7) The organic phase was shaken with 10 ml. of water containing sufficient solid hydroxylamine hydrochloride present to decolourise the ether/benzene.

(8) The aqueous phase containing antimony(III) was digested on a water-bath with an equal volume of a saturated ammonium thiocyanate solution. The red antimony(III) sulphide

precipitate was transferred to a filter-disc, washed with water and acetone and dried at 120°C.

Iodine

Carrier solution

Potassium iodide was dissolved in water and standardised by precipitations as palladium(II) iodide.

Separation from 2 gm. of uranyl nitrate

(1) The uranyl nitrate was dissolved in 20 ml. of 2 M hydrochloric acid in a 100 ml. beaker. 5 ml. of concentrated ammonia were added followed by carrier solutions containing the elements to be separated.

(2) The mixture was warmed with sufficient saturated sodium carbonate solution to dissolve precipitated uranium oxides. 2 ml. of a 2% solution of sodium hypochlorite were added and the solution was set aside for ten minutes.

(3) It was then transferred to a 250 ml. separating funnel containing 20 ml. of carbon tetrachloride. The aqueous solution was acidified by the dropwise addition of concentrated nitric acid. 5 ml. of a 10% solution of hydroxylamine hydrochloride were added and the liberated iodine transferred into the carbon tetrachloride by shaking.

(4) The iodine was back-extracted as iodide into 5 ml. of water containing 3 drops of a saturated sulphur dioxide solution.

(5) The aqueous phase containing a few drops of nitric acid and three drops of sodium nitrite solution was shaken with 5 ml. of carbon tetrachloride.

(6) The iodine was again extracted into 5 ml. of water containing 2 drops of sulphur dioxide solution. A slight excess of palladium nitrate solution was added and the palladium(II) iodide which precipitated was transferred to a filter-disc, washed with water and acetone and dried at 120°C.

Separation Procedure for 10 gm. of Uranyl Nitrate

(1) The mixture of uranyl nitrate and the carrier solutions were diluted to 20 ml. so that the solution was 6 M in hydrochloric acid. One ml. of 1 M sodium chlorate solution was added and the iodine monochloride produced was extracted into 20 ml. of n-butyl acetate.

(2) The butyl acetate phase was shaken with 5 ml. of water containing 3 drops of a saturated sulphur dioxide solution and the organic phase was discarded.

(3) Steps (5) and (6) of the previous method were then carried out.

Cerium

Carrier solution

Cerium(III) chloride was dissolved in 2 M hydrochloric acid and the solution was standardised titrimetrically using EDTA and Xylenol Orange indicator at pH 5.6 - 6.0.

Separation Procedure

(1) To the uranyl nitrate dissolved in 2 M hydrochloric acid were added carriers for the elements to be separated. The solution was boiled after the addition of 2 drops of bromine followed by 2 ml. of hydroxylamine hydrochloride solution.

(2) Cerium(III) fluoride was precipitated by transferring the solution to a polyethylene centrifuge tube adding 2 ml. of concentrated hydrofluoric acid and digesting for 10 minutes.

(3) The cerium(III) fluoride precipitate was dissolved in 2 ml. each of saturated boric acid and concentrated nitric acid by warming. After diluting to 10 ml. with water, cerium

fluoride was precipitated as in step (2).

(4) The cerium(III) fluoride precipitate was dissolved using boric and nitric acid as in step (2) and the solution was made 4 M in nitric acid.

(5) The cerium(III) solution was transferred to a separating funnel and shaken twice, each time for 2 minutes, with 20 ml. of a 0.1 M solution of HDEHP in carbon tetrachloride. The organic phases were discarded and the aqueous solution was shaken with 20 ml. of carbon tetrachloride which was in turn discarded.

(6) 4 ml. of 1 M potassium bromate solution and 2 ml. of concentrated nitric acid were added to the aqueous phase which was then shaken with 20 ml. of 0.1 M HDEHP in petroleum ether.

(7) The aqueous phase was tested for cerium by the addition of a concentrated ammonia solution and if free from it, it was discarded. The organic phase was washed three times with 10 ml. of 4 M nitric acid, then with 10 ml. of 0.5 nitric acid and the washes discarded.

(7) Cerium was back-extracted by shaking the petroleum ether phase twice with 10 ml. of 0.5 M nitric acid containing

a few drops of 30% hydrogen peroxide. The aqueous extracts were made alkaline using concentrated ammonia solution and heated in a water-bath to destroy the hydrogen peroxide. (8) Cerium hydroxide was collected by centrifugation, taken up in 6 drops of 6 M hydrochloric acid solution, diluted to 10 ml. with water and digested for 5 minutes with 5 ml. of saturated oxalic acid. The cerium(III) oxalate was transferred to a filter disc, washed with ethanol and ether and dried under vacuum.

Analysis of the Sources

The filter-disc containing the cerium(III) oxalate precipitate was transferred to a 250 ml. flask and warmed with 5 ml. of 4 M nitric acid to dissolve the precipitate. The solution was diluted to 50 ml. and 3 ml. of a 20% solution of ammonium persulphate was added. The solution was boiled until the Ce IV colour appeared, a small crystal of hydroxylamine hydrochloride was added and the solution was cooled. The pH was adjusted to 5.6 - 6.0 and the solution was titrated using 0.01 M EDTA and Xylenol Orange indicator.

Praesodymium

Carrier solution

Praesodymium oxide was dissolved in concentrated hydrochloric acid and diluted with water. The solution was standardised by titration with EDTA using Xylenol Orange indicator.

Separation Procedure

The identical procedure outlined for yttrium was followed for praesodymium recovery. Praesodymium was eluted approximately 2 hours after yttrium. The main fractions were collected as oxalate and transferred to a filter-disc.

Analysis of sources

The praesodymium sources were analysed by the method described for cerium.

Appendix B

Least-Squares program to fit single component decays.

Language: Elliot Algol

```
BEGIN       INTEGER  I, K, RUN, N;
            READ N;
BEGIN REAL  LAMI, AIO, TI, C, VARO, STDEVA, STEVB, DA,
DB, B11, B12, B22, D11, D12, D22, C1, C2, C3, S, VAREX,
DENOM;
            ARRAY  A, T, FO, FT, FA1O, FC, L,
EXTRA, TOTA (1 : N);
            SWITCH SS:= CYCLE, FINISH;
            REAL PROCEDURE SUM (F1, F2);
            ARRAY  F1, F2;
            BEGIN REAL  S; INTEGER J;
            S:= 0;
            FOR J:=  1 STEP 1 UNTIL N DO
            S: = S + F1 (J) * F2 (J) / L(J);
            SUM: = S;
            END OF SUM;
```

```
READ  RUN, T1, A10, C, VARO;
PRINT  £
RUN NUMBER?, SAMELINE, DIGITS (3), RUN,£
    HALFLIFE = ?, FREEPOINT (4), T1;
FOR I: = 1 STEP 1 UNTIL N DO
READ T(I), A(I), TOTA(I);
LAMI: = 0.9315 / T1;
CYCLE: FOR I: = 1 STEP 1 UNTIL N DO BEGIN
EXTRA(I): = EXP(-LAMI * T(I));
   FO(I): = A(I) - A10 * EXTRA(I) - C;
   FT(I): = LAMI * A10 * EXTRA(I);
 FA10(I): = -EXTRA(I);
   FC(I): = -1;
    L(I): = A(I) * A(I) / TOTA(I); END;
      K : = K + 1;
     B11: = SUM(FA10, FA10);
     B12: = SUM(FA10, FC);
     B22: = SUM(FC, FC);
   DENOM: = B11 * B22 - B12 * B12;
      C1: = SUM(FO, FA10);
      C2: = SUM(FO, FC);
```

```
        D11: = B22 / DENOM;
        D12: =-B12 / DENOM;
        D22: = B11 / DENOM;
         DA: = D11 * C1 - D12 * C2;
         DB: = D12 * C1 - D22 * C2;
        A10: = A10 - DA;
          C: = C   - DB;
    IF  ABS(DA/A10) LESSEQ 1@- 4 THEN GO TO FINISH;
    IF  ABS(DB/C)   LESSEQ 1@- 4 THEN GO TO FINISH;
    IF  K GREQ 15 THEN GO TO FINISH ELSE GO TO CYCLE;
FINISH:
        S: = 0;
     FOR I: = 1 STEP 1 UNTIL N DO
        S: = S + FO(I) * FO(I);
     VAREX: = S / (N - 2);
    PRINT  ££L2?  S =£ S??, SAMELINE, S, ££S2?, VAREX = ?,
                                                    VAREX;
    STDEVA: = SQRT (D11 * VAREX);
    STDEVB: = SQRT (D22 * VAREX);
```

```
FOR I: = 1 STEP 1 UNTIL N DO BEGIN
IF ABS(FO(I) / A(I))  GR .03 THEN PRINT £
REJECT POINT, T = ?, SAMELINE, T(I), £A = ?, A(I),
 £RESIDUAL = ?, FO(I);                              END;
PRINT £
TIME £S2? LS. ACTIVITY £S4? OBS. ACTIVITY £S2? EXPONENTIAL
                                                    £L2 ??;
FOR I: = 1 STEP 1 UNTIL N DO BEGIN
PRINT FREEPOINT(4), T(I), PREFIX( ££S4??), ALIGNED(5, 1),
A10 * EXP(-LAMI * T(I)) + C, A(I), FREEPOINT (4),
EXP(-LAMI * T(I));                                  END;
PRINT £
A10 = £S2??, SAMELINE, A,  ££S3?  ST DEVN A10 = ?,
STDEVA, ££L2?  RESID. ACTIVITY, C = ?, SAMELINE, C,
 ££S3? STDEVN C = ?, STEVB, ££L2? TOTAL MATRIX B = ?,
SCALED(4), DENOM;
END; END; END;
```

References

Chapter 1

1.1 E. Fermi, Nature 133, 898 (1934).

1.2 O. Hahn and F. Strassman, Naturwiss 27, 11 (1939).

1.3 O. Hahn and F. Strassman, Naturwiss 27, 529 (1939).

1.4 L. Meitner and O.R. Frisch, Nature 143, 239 (1939).

1.5 L.A. Turner, Rev. Mod. Phys. 12, 1 (1940).

1.6 C.D. Coryell and N. Sugarman (editors), 'Radiochemical Studies; The Fission Products', N.N.E.S., Div. IV, Vol. 9.

1.7 N. Bohr and J. Wheeler, Phys, Rev., 56, 426 (1939).

1.8 J. Fenkel, Phys. Rev., 55, 987 (1939).

1.9 G.N. Walton, Quarterly Reviews, 15, 71 (1961).

1.10 I. Halpern, Ann. Rev. Nuc. Sci., 9. 245 (1959).

1.11 E.K. Hyde, 'The Nuclear Properties of the Heavy Elements; pt. III, Fission Phenomena', (1964).

1.12 U.N. 2nd Conference on the Peaceful Uses of Atomic Energy. (1958).

1.13 N. Bohr, Phys. Rev., 55, 418 (1939).

1.14 R.E. Batzel and G. T. Seaborg, Phys. Rev. 82, 607 (1951).

1.15 G.T. Seaborg, Phys. Rev., 88, 1429 (1952).

1.16 G.N. Flerov, D.S. Klochkov, V.S. Skobkin and V.V. Terent'ev, Sov. Phys.(Doklady) 3, 79 (1958).

1.17 E. Segre, Phys. Rev. 86, 21 (1952).

1.18 R. Vandenbosch, P.R. Fields, S.E. Vandenbosch and D. Metta, J.I.N.C., 26, 219 (1964).

1.19 G.R. Choppin, Phys. Rev. 98, 1519 (1955).

1.20 R.O. Haxby, W.E. Shoupp, W.E. Stephens and W.A. Wells, Phys. Rev. 59, 57 (1941).

1.21 T. Sikkeland, S.G. Thompson and E. Ghiorso, Phys. Rev. 112, 543 (1958).

1.22 E.W. Titterton, Nature 168, 590 (1951).

1.23 D.L. Hill and J. A. Wheeler, Phys. Rev. 89, 1102 (1953).

1.24 E.C. Albenesius, Phys. Rev. Lett. 3, 274 (1959).

1.25 E.C. Albenesius and R.S. Ondejcin, Nucleonics 18, 100 (1960).

1.26 L. Rosen and A. M. Hudson, Phys. Rev. 78, 533 (1950).

1.27 L.E. Glendenin, C.D. Coryell and G.W. Edwards, paper 52 of ref. 1.6.

1.28 A.C. Pappas, Proceedings of the U.N. Conference on the Peaceful Uses of Atomic Energy, 7, P/881 (1955).

1.29 T.J. Kennett and H.G. Thode, Phys. Rev. 103, 323 (1956).

1.30 A.C. Wahl, J.I.N.C. 6, 263 (1958).

1.31 S. Katcoff, Nucleonics 18, 201 (1960).

1.32 W. Jentschke and F. Frankl, Naturwiss 27, 134 (1939).

1.33 E.P. Steinberg and L.E. Glendenin, Phys. Rev. 95, 431 (1954).

1.34 W.E. Nervik, Phys. Rev. 119, 1685 (1960).

1.35 P.C. Stevenson, H.G. Hicks, W.E. Nervik and D.R. Nethaway, Phys. Rev. 111, 886 (1958).

1.36 A.W. Fairhall, Phys. Rev. 102, 1335 (1957).

1.37 R.H. Goeckerman and I. Perlman, Phys. Rev. 76, 628 (1949).

1.38 R.C. Jensen and A.W. Fairhall, Phys. Rev., 109 942 (1958).

1.39 L.J. Colby, M. la Salle-Shoaf and J. Cobble, Phys. Rev. 121, 1415 (1961).

1.40 R.H. Iyer, C.K. Mathews, N. Ravindran, K. Rengan, D.V. Singh, M.V. Ramaniah and H.D. Sharma, J.I.N.C. 25, 465 (1963).

1.41 M.G. Brown, Ph.D. Thesis. Durham (1966).

1.42 V.F. Apalin, Yu. N. Gritsyuk, I.E. Kutikov, V.I. Lebedev and L.A. Mikaelian, Nucl. Phys 71, 546 (1965).

1.43 J. Milton and J. Fraser, Phys. Rev. Lett. 7, 67 (1961).

1.44 J. Milton and J. Fraser, Can J. Phys. 40, 1626 (1962).

1.45 J. Terrell, Phys. Rev. 127, 380 (1962).

1.46 V.F. Apalin, Y.N. Gritsyuk, I.E. Kutikov, V.I. Lebedev, and L.A. Mikaelian, Nucl. Phys. 55, 249 (1958).

1.47 V.F. Apalin, Yu.N. Gritsyuk, I.E. Kutikov, V.I. Lebedev, L.A. Mikaelian and L.A. Kurchatov, Nucl. Phys. 71, 553 (1965).

1.48 W.E. Stein and S.L. Whetstone, Jr., Phys. Rev. 110, 476 (1958).

1.49 J.C.D. Milton and J.S. Fraser, AECL-2163 (Feb. 1965).

1.50 H.G. Thode and R.L. Graham, Can. J. Research 25A, 1 (1947).

1.51 R.K. Wanless and H.G. Thode, Can. J. Phys. 33, 541 (1955).

1.52 A.C. Wahl, Phys. Rev. 99, 730 (1955).

1.53 A. Hemmendinger, Paper 663 in reference 1.12.

1.54 L.E. Glendenin, Phys. Rev. 75, 337 (1949).

1.55 Wiles, Smith, Horsley and Thode, Can. J. Phys. 31, 419 (1953).

1.56 H. Farrar and R.H. Tomlinson, Can. J. Phys. 40, 943 (1963).

1.57 R. Ramanna, R. Subramanian and R.N. Iyer, Nucl. Phys. 67, 529 (1965).

1.58 W.J. Swiatecki, Proceedings of the Symposium on the Physics and Chemistry of Fission. Salzburg 1965, P.3.

1.59 P. Fong, Phys. Rev. 102, 434 (1956).

1.60 A. Bohr, Paper 157 of Reference 1.12.

1.61 H. Faissner and K. Wildermuth, Nucl. Phys. 58, 177 (1964).

1.62 R. Vandenbosch, Nucl. Phys. 58, 177 (1964).

1.63 L. Meitner, Nature 165, 561 (1950).

1.64 W.H. Walker, A.E.C.L.-1537 (1962).

1.65 E.K. Bonyushkin, Yu. S. Zamatin, I.S. Kirin, W.P. Martynov, E.K. Skvortsov and V.N. Ushatskii, A.E.C.-tr-4682.

1.66 K.A. Petrzhak, G.M. Tolmachev, V.N. Ushatskii, M.A. Bak, N.I. Blinova and S.S. Bugorkov A.E.C.-tr-4696.

Chapter 2

2.1 C.G.B. Williams, Ph.D. Thesis, Durham (1966).

2.2 B.W. East, Ph.D. Thesis, Durham (1967).

2.3 Md. M. Rahman, Ph.D. Thesis, Durham (1966).

2.4 E.J. Wilson and C. Evans, Atomics 9, 238 (1958).

2.5 R.H. James, G.R. Martin and D.J. Silvester, Radiochimica Acta, 3, 76 (1964).

2.6 R.I. Chase & W.A. Higinbotham, Rev. Sci. Insti. 23, 34 (1952).

2.7 K. Kandish, Proc. Inst. Elect. Eng 101 part II 239 (1954).

2.8 B.D. Pate & L. Yaffe, Can. J. Chem. 33, 929 (1955)

2.9 B.P. Bayhurst & R.J. Prestwood, Nucleonics 17 82 (1959).

2.10 Reference 1,41.

Chapter 3

3.1 V.G. Hermann, Radiochim. Acta 3, 169 (1964).

3.2 Procedure 2 in 'The Radiochemistry of Zirconium and Hafnium', NAS-NS 3011.

3.3 E.S. Pilkington and W. Wilson, Anal. Chim. Acta, 33, 577 (1965).

3.4 Reference 1.64.

3.5 Reference 1.65.

3.6 Reference 1.66.

3.7 C.W. Stanley, Procedure Y/4 in "The Radiochemistry of the rare earths", NAS-NS 3020.

3.8 S.J. Lyle and Md. M. Rahman, Talanta 10, 1183 (1963).

3.9 J. Walczynska, Chemia Analityczna 6, 969 (1961).

3.10 N.E. Ballou, N.N.E.S. Div. IV vol. 9.

3.11 W.J. Maeck, M.E. Kussy and J.E. Rein, Anal. Chem. 33, 237 (1961).

3.12 Procedure 3 in "The Radiochemistry of Rhodium" NAS-NS 3008.

3.13 Procedure 2 in NAS-NS 3008.

3.14 F.E. Beamish, 'The Analytical Chemistry of the Noble Metals', Pergamon Press (1966).

3.15 J. Murandat and C. Duval, Analyt. Chim. Acta. 4, 498 (1950).

3.16 Reference 2.10.

3.17 O. Birgul, Private Communication.

3.18 W.W. Meinke, A.E.C.D. - 2738.

3.19 A.I. Vogel, 'A Textbook of Quantitative Analysis', p 568.

3.20 'Radiochemical Purification for the Elements', Compiled by M. Lindner, U.C.R.L. - 14258.

3.21 'The Radiochemistry of the Rare Earths', NAS-NS 3020.

3.22 D.F. Peppard, S.W. Moline and G.W. Mason, J.I.N.C. 4, 344 (1957).

3.23 F.D. Snell and C.T. Snell, 'Colorimetrical Methods of Analysis', Van Nostrand (1949) p 607.

3.24 W.E. Nervik, Procedure RE/1 in "The Radiochemistry of the rare earths", NAS-NS 3020.

Chapter 4

4.1 L. Salmon, A.E.R.E. - R 3640.

4.2 W.E. Nervik, Paper 1-2 in "Applications of Computers to Nuclear and Radiochemistry", NAS-NS 3107.

4.3 R.D. Evans, "The Atomic Nucleus", McGraw-Hill (1955), p.752.

4.4 W.E. Wentworth, J. Chem. Ed., 42, 96 (1965).

4.5 W.E. Deming, "Statistical Adjustment of Data", John Wiley and Sons, Inc., New York 1943.

Chapter 5

5.1 C.D. Coryell, Ann. Rev. Nuc. Sci., 2, 305 (1953).

5.2 A.C. Wahl, J.I.N.C., 6, 263 (1958).

5.3 R.B. Leachman, (P/665), 2nd U.N. Conf. P.U.A.E., Geneva (1958).

5.4 W.H. Walker, A.E.C.L.-1537 (1962).

5.5 E.K. Bonyushkin, Yu. S. Zamatin, I.S. Kirin, W.P. Martynov, E.K. Skvortsov and V.N. Ushatskii, A.E.C.-tr-4682.

5.6 K.A. Petrzhak, G.M. Tolmachev, V.N. Ushatskii, M.A. Bak, N.I. Blinova and S.S. Burgorkov, A.E.C.-tr-4696.

5.7 R.H. James, G.R. Martin, D.J. Silvester, Radiochim. Acta, 3, 76 (1964).

5.8 K.M. Broom, Phys. Rev., 127, 637 (1962).

5.9 A.N. Protopopov, M.I. Kuznetsov and E.G. Dermenzhiev, Sov. Phys. J.E.T.P., 9, 1374 (1959).

5.10 J.G. Cuninghame, J.I.N.C., 5, 1 (1957).

5.11 G.P. Ford, J.S. Gilmore and D.P. Ames, LA-1997 (1956).

5.12 Md. M. Rahman, Ph.D. Thesis, Durham (1966).

5.13 V.F. Apalin, Y.N. Gritzyuk, I.Y. Kutikov, V.I. Lebeder and L.A. Mikaelyan, Nucl. Phys., 38, 193 (1962).

5.14 J.S. Fraser and J.C.D. Milton, Phys. Rev., 93, 818 (1954).

5.15 S.L. Whetstone, Jr., Phys. Rev., 114, 581 (1959).

5.16 J. Terrell, Proc. Int. Symp. on the Phys. and Chem. of Fission, Volume 2 (Salzburg, 1965).

5.17 M.J. Bennett and W.E. Stein, Phys. Rev., 156, 1277 (1967).

5.18 E. Cheifetz and Z. Fraenkel, Phys. Rev. Lett., 21, 36 (1968).

5.19 H.B. Levy, H.G. Hicks, W.E. Nervik, P.C. Stevenson, J.B. Niday and J.C. Armstrong, Jr., Phys. Rev., 124, 544 (1961).

5.20 L.R. Bunney, E.M. Scadden, J.O. Abriam and N.E. Ballou, (P/643), 2nd U.N. Conf. P.U.A.E. (1958).

5.21 R.N. Keller, E.P. Steinberg and L.E. Glendenin, Phys. Rev., 94, 969 (1954).

5.22 D.J. Gorman and R.H. Tomlinson, Can. J. Chem., 46, 1663 (1968).

5.23 S.C. Burnett, R.L. Ferguson, F. Plasil and H.W. Schmitt, Phys. Rev. Lett., 21, 1350 (1968).

5.24 R. Vandenbosch, Nucl. Phys., 46, 129 (1963).

5.25 H. Faissner and K. Wildermuth, Nucl. Phys., 58, 177 (1964).

5.26 S.J. Lyle, G.R. Martin and Md. M. Rahman, Radiochim. Acta., 9, 90 (1968).